Atmos. Meas. Tech., 8, 4947–4977, 2015
www.atmos-meas-tech.net/8/4947/2015/
doi:10.5194/amt-8-4947-2015

Atmospheric Measurement Techniques
Open Access
EGU

Evaluation of the operational Aerosol Layer Height retrieval algorithm for Sentinel-5 Precursor: application to O_2 A band observations from GOME-2A

A. F. J. Sanders[1,a], J. F. de Haan[1], M. Sneep[1], A. Apituley[1], P. Stammes[1], M. O. Vieitez[1], L. G. Tilstra[1], O. N. E. Tuinder[1], C. E. Koning[1], and J. P. Veefkind[1]

[1]Royal Netherlands Meteorological Institute, De Bilt, the Netherlands
[a]now at: Institute of Environmental Physics, University of Bremen, Bremen, Germany

Correspondence to: A. F. J. Sanders (asanders@uni-bremen.de)

Received: 11 May 2015 – Published in Atmos. Meas. Tech. Discuss.: 19 June 2015
Revised: 2 October 2015 – Accepted: 10 November 2015 – Published: 25 November 2015

Abstract. An algorithm setup for the operational Aerosol Layer Height product for TROPOMI on the Sentinel-5 Precursor mission is described and discussed, applied to GOME-2A data, and evaluated with lidar measurements. The algorithm makes a spectral fit of reflectance at the O_2 A band in the near-infrared and the fit window runs from 758 to 770 nm. The aerosol profile is parameterised by a scattering layer with constant aerosol volume extinction coefficient and aerosol single scattering albedo and with a fixed pressure thickness. The algorithm's target parameter is the height of this layer. In this paper, we apply the algorithm to observations from GOME-2A in a number of systematic and extensive case studies, and we compare retrieved aerosol layer heights with lidar measurements. Aerosol scenes cover various aerosol types, both elevated and boundary layer aerosols, and land and sea surfaces. The aerosol optical thicknesses for these scenes are relatively moderate. Retrieval experiments with GOME-2A spectra are used to investigate various sensitivities, in which particular attention is given to the role of the surface albedo.

From retrieval simulations with the single-layer model, we learn that the surface albedo should be a fit parameter when retrieving aerosol layer height from the O_2 A band. Current uncertainties in surface albedo climatologies cause biases and non-convergences when the surface albedo is fixed in the retrieval. Biases disappear and convergence improves when the surface albedo is fitted, while precision of retrieved aerosol layer pressure is still largely within requirement levels. Moreover, we show that fitting the surface albedo helps to ameliorate biases in retrieved aerosol layer height when the assumed aerosol model is inaccurate. Subsequent retrievals with GOME-2A spectra confirm that convergence is better when the surface albedo is retrieved simultaneously with aerosol parameters. However, retrieved aerosol layer pressures are systematically low (i.e., layer high in the atmosphere) to the extent that retrieved values no longer realistically represent actual extinction profiles. When the surface albedo is fixed in retrievals with GOME-2A spectra, convergence deteriorates as expected, but retrieved aerosol layer pressures become much higher (i.e., layer lower in atmosphere). The comparison with lidar measurements indicates that retrieved aerosol layer heights are indeed representative of the underlying profile in that case. Finally, subsequent retrieval simulations with two-layer aerosol profiles show that a model error in the assumed profile (two layers in the simulation but only one in the retrieval) is partly absorbed by the surface albedo when this parameter is fitted. This is expected in view of the correlations between errors in fit parameters and the effect is relatively small for elevated layers (less than 100 hPa). If one of the scattering layers is near the surface (boundary layer aerosols), the effect becomes surprisingly large, in such a way that the retrieved height of the single layer is above the two-layer profile.

Furthermore, we find that the retrieval solution, once retrieval converges, hardly depends on the starting values for the fit. Sensitivity experiments with GOME-2A spectra also show that aerosol layer height is indeed relatively robust against inaccuracies in the assumed aerosol model, even when the surface albedo is not fitted. We show spectral fit residuals, which can be used for further investigations. Fit

residuals may be partly explained by spectroscopic uncertainties, which is suggested by an experiment showing the improvement of convergence when the absorption cross section is scaled in agreement with Butz et al. (2013) and Crisp et al. (2012), and a temperature offset to the a priori ECMWF temperature profile is fitted. Retrieved temperature offsets are always negative and quite large (ranging between -4 and -8 K), which is not expected if temperature offsets absorb remaining inaccuracies in meteorological data. Other sensitivity experiments investigate fitting of stray light and fluorescence emissions. We find negative radiance offsets and negative fluorescence emissions, also for non-vegetated areas, but from the results it is not clear whether fitting these parameters improves the retrieval.

Based on the present results, the operational baseline for the Aerosol Layer Height product currently will not fit the surface albedo. The product will be particularly suited for elevated, optically thick aerosol layers. In addition to its scientific value in climate research, anticipated applications of the product for TROPOMI are providing aerosol height information for aviation safety and improving interpretation of the Absorbing Aerosol Index.

1 Introduction

Preparations are currently being made to operationally retrieve aerosol properties from absorption of reflected sunlight by oxygen in its A band around 760 nm (e.g., ESA, 2012; Fishman et al., 2012). Building upon the long heritage of cloud retrieval from the O_2 A band, aerosol retrieval is a similar problem, but it is more challenging because of the variability in particle microphysical properties and the much lower particle optical thickness (typically 1–2 orders of magnitude). Because of the latter, the contribution of aerosols to the top-of-atmosphere reflectance is much smaller and approximate methods that rely on a large multiple scattering contribution (e.g., Lambertian surface as a cloud model, asymptotic solutions of the radiative transfer equations) cannot be used in the case of aerosol retrieval. In this paper, we describe and discuss a retrieval setup for retrieval of aerosol height with the TROPOspheric Monitoring Instrument (TROPOMI) on the Sentinel-5 Precursor mission (Veefkind et al., 2012). We evaluate the algorithm by applying it to observations from the Global Ozone Monitoring Experiment-2 (GOME-2) instrument on the Meteorological Operational satellite-A (Metop-A) platform in a series of extensive case studies.

A number of operational satellite cloud retrieval schemes are based on spectral measurements of the O_2 A band. These include the Fast REtrieval Scheme for Clouds from the Oxygen A band (FRESCO), the Semi-Analytical CloUd Retrieval Algorithm (SACURA), and Retrieval Of Cloud Information using Neural Networks (ROCINN). The main characteristics of each retrieval scheme are given in Table 1. Note that in all three retrieval setups, (i) the assumed cloud profile is a scattering layer with constant particle volume extinction coefficient or an isotropically reflecting surface, (ii) the cloud covers the ground pixel with a particular cloud fraction, and (iii) the ground surface albedo is taken from climatologies and fixed in retrieval. Much experience with application of these retrieval schemes to various satellite instruments (GOME-2, GOME: Global Ozone Monitoring Experiment, SCIAMACHY: SCanning Imaging Absorption spectroMeter for Atmospheric CHartographY) has been built up over the past years (e.g., Lelli et al., 2012, 2014; Wang and Stammes, 2014; Wang et al., 2008; Loyola et al., 2007; Kokhanovsky et al., 2006a, b; Koelemeijer et al., 2001, 2002).

Various instrument requirement and sensitivity studies investigating the potential of spectral measurements of the O_2 A band for aerosol retrieval have appeared in the past. These studies include the ones by Geddes and Bösch (2015), Hollstein and Fischer (2014), Sanders and De Haan (2013), Hollstein et al. (2012), Hasekamp and Sidans (2009), Siddans et al. (2007), Corradini and Cervino (2006), and Gabella et al. (1999). Overall, these studies show, among other things, that retrieval precision is typically better when the aerosols are optically thicker or more elevated, or when the solar zenith angle is larger. The amount of aerosol profile information from such a passive satellite measurement is, however, limited (Geddes and Bösch, 2015; Corradini and Cervino, 2006; Timofeyev et al., 1995).

Case studies based on satellite data have been performed by Koppers and Murtagh (1997) for GOME data, and by Sanghavi et al. (2012) and Kokhanovsky and Rozanov (2010) for SCIAMACHY data. Koppers and Murtagh (1997) show retrieved aerosol optical thickness from GOME for 2 months of global observations and for several months of observations over two AErosol RObotic NETwork (AERONET) stations near the Saharan desert. Sanghavi et al. (2012) analyse retrievals for a year of SCIAMACHY observations over an AERONET station in the Indo–Gangetic Plain, and Kokhanovsky and Rozanov (2010) demonstrate their retrieval technique using a SCIAMACHY observation of a Saharan dust outbreak over the Atlantic Ocean. Koppers and Murtagh (1997) fit aerosol optical depth in five atmospheric layers, Sanghavi et al. (2012) parameterise the aerosol extinction profile by a lognormal function for which they retrieve the peak height and the width in addition to optical thickness, while Kokhanovsky and Rozanov (2010) fit the optical thickness and the top of a scattering layer that extends to the ground and has a constant aerosol volume extinction coefficient inside the layer. Only in the retrieval scheme proposed by Koppers and Murtagh (1997) is the surface albedo retrieved simultaneously with aerosol parameters. The issue of selecting cloud-free pixels is explicitly addressed by Koppers and Murtagh (1997), who devised a cloud mask based on sub-pixel information from GOME's polarisation measure-

Table 1. Characteristics of operational satellite cloud retrieval schemes using spectral measurements of the O_2 A band.

Retrieval scheme	Satellite instruments	Cloud model	Cloud fraction	Surface albedo	References
Fast REtrieval Scheme for Clouds from the Oxygen A band (FRESCO)	Global Ozone Monitoring Experiment-2 (GOME-2), Global Ozone Monitoring Experiment (GOME), SCanning Imaging Absorption spectroMeter for Atmospheric CHartography (SCIAMACHY)	Lambertian surface with albedo of 0.8; the height of the Lambertian surface is a fit parameter.	Cloud fraction is a fit parameter.	From climatology	Wang et al. (2008); Koelemeijer et al. (2001)
Semi-Analytical CloUd Retrieval Algorithm (SACURA)/ SACURA – Next Generation for GOME (SNGome)	GOME-2, GOME, SCIAMACHY	Scattering layer with constant particle volume extinction coefficient; cloud top height, cloud geometrical thickness and cloud optical thickness are fit parameters.	Cloud fraction is determined from an analysis of the polarisation measurement devices' (PMDs) broadband reflectances (OCRA: Optical Cloud Recognition Algorithm; Loyola et al., 2007) and used as an input for retrieval.	From climatology	Kokhanovsky and Rozanov (2004); Rozanov and Kokhanovsky (2004)
Retrieval Of Cloud Information using Neural Networks (ROCINN)	GOME-2, GOME	Lambertian surface; the albedo and the height of the Lambertian surface are fit parameters.	Cloud fraction is determined from an analysis of PMD broadband reflectances (OCRA; Loyola et al., 2007) and used as an input for retrieval.	From climatology	Loyola et al. (2007)

ment devices (PMDs). Kokhanovsky and Rozanov (2010) use visual inspection of a MEdium Resolution Imaging Spectrometer's (MERIS) RGB image to select a cloud-free SCIAMACHY pixel and Sanghavi et al. (2012) dissociate aerosols from clouds in a post-retrieval analysis of retrieved optical thickness. Finally, a comparison of retrieved aerosol optical thickness with AERONET aerosol optical thickness is provided by Koppers and Murtagh (1997) and Sanghavi et al. (2012). None of these studies compared the retrieved height distribution with independent measurements.

This brief summary of previous case studies already illustrates a number of issues involved when setting up an O_2 A band aerosol retrieval: the choice of the vertical profile assumed in retrieval, masking of pixels containing clouds, and validation of the retrieval results. We continue these case studies using data from GOME-2A. Our primary goal is to retrieve aerosol layer height (see below). Based on the case studies discussed above and on our own experiences, we pay special attention to the following three aspects when setting up the experiments. Firstly, we put effort in accurate cloud masking and in cirrus masking in particular. Even though cirrus clouds are optically thin, their optical thickness is similar in magnitude to aerosol optical thicknesses and, as a consequence, any undetected cirrus may significantly bias retrieved aerosol height (e.g., Sanders and De Haan, 2014; see also Sect. 10 of this paper). We use an Advanced Very High Resolution Radiometer (AVHRR) cloud mask accurately collocated to the respective GOME-2A pixel that includes a dedicated cirrus test using AVHRR's thermal infrared channels. Secondly, we apply our algorithm to observations of aerosol scenes covering different aerosol types and height distributions as well as covering sea and land surfaces. The aerosol scenes concern desert dust near the coast of West Africa and over the Iberian Peninsula, volcanic ash over Europe, smoke from forest fires in North America transported across the Atlantic Ocean, aerosols over the Aegean Sea, and various boundary layer aerosol and multi-layered aerosol cases over the Netherlands. We select this set of aerosol scenes to assess the algorithm's performance under different aerosol and surface conditions. Thirdly, we select aerosol scenes for which a lidar measurement (ground-based, airborne or space-borne) is available for at least one ground pixel in the scene. A proper understanding and evaluation of the retrieved aerosol height parameter is not possible without independent measurements of the actual aerosol extinction profile.

Our retrieval setup can be briefly described as follows. A spectral fit of reflectances across the O_2 A band from 758 to 770 nm is made. We do not retrieve a full extinction profile

but limit ourselves to retrieving only one height parameter because of the limited information content. We parameterise the aerosol profile by a single layer of particles with a constant particle volume extinction coefficient and particle single scattering albedo and with a fixed pressure thickness (i.e., the pressure difference between the top and the bottom of the layer is fixed). Then, we retrieve and report the mid pressure of the assumed aerosol layer (top pressure plus bottom pressure divided by two). This parameterisation comes closest to the parameterisation employed by SACURA. Note that FRESCO and ROCINN retrieve only one cloud height parameter too. In addition to mid pressure, we also retrieve the aerosol layer's optical thickness and, depending on the experimental condition, the surface albedo. Since the contribution of aerosols to the top-of-atmosphere reflectance is small, the surface has a relatively large contribution. In Sect. 2 we will argue, based on a simulation study, that uncertainties in current surface albedo climatologies lead to significantly biased and non-convergent retrievals of aerosol properties from the O_2 A band when the surface albedo is treated as a fixed model parameter. This is one of the reasons why in one of the experimental conditions for the GOME-2A retrievals we also fit the surface albedo (as opposed to, for example, the cloud retrieval schemes mentioned above). We will come back to the point of fitting the surface albedo and the effect it has on the retrieval outcome in the remainder of this paper. Finally, we assume the aerosol layer to fully cover the target pixel (aerosol fraction of one). There is only very little information available in the O_2 A band for simultaneously retrieving aerosol/cloud optical thickness and aerosol/cloud fraction (e.g., Van Diedenhoven et al., 2007). Note that in the operational cloud retrieval schemes discussed above one of the two parameters is indeed fixed or retrieved in a separate step.

The work presented in this paper is part of an on-going effort to develop a dedicated Aerosol Layer Height (ALH) product for TROPOMI on the Sentinel-5 Precursor mission. Its main purpose is to retrieve and report the height of (vertically localised) aerosol layers in the free troposphere, such as desert dust, biomass burning aerosols and volcanic ash plumes. Observations of aerosol height are of scientific interest, for example, for improving estimates of injection heights for transport modelling, for calculating direct radiative effects, or for better understanding effects on local atmospheric stability related to aerosol absorption. An important intended application of the TROPOMI product is providing aerosol height information for aviation safety. Furthermore, aerosol height information can be used to improve interpretation of the Absorbing Aerosol Index (AAI; De Graaf et al., 2005), as this index is strongly height-dependent. Currently, Aerosol Layer Height and Absorbing Aerosol Index are the two operational TROPOMI aerosol products. Science requirements for the Aerosol Layer Height product are defined in Van Weele et al. (2008). The target requirement on accuracy and precision of retrieved aerosol layer height is 0.5 km or 50 hPa; the threshold requirement is 1 km or 100 hPa. A minimum aerosol optical thickness for which these requirements should be met is not indicated. Also note that requirements are not specified for the accuracy and precision of retrieved aerosol optical thickness from the O_2 A band. Dedicated retrievals of spectral aerosol optical thickness are provided by separate algorithms foreseen for TROPOMI or already operational for the Visible Infrared Imaging Radiometer Suite (VIIRS) on the Suomi National Polar-orbiting Partnership (Suomi NPP) mission. (TROPOMI is planned to fly in loose formation with Suomi NPP.) These aerosol optical thickness retrievals typically cover wavelength ranges that are much broader than the fit window used in our O_2 A band retrieval (currently 12 nm). The Algorithm Theoretical Basis Document for the Aerosol Layer Height product has been delivered as Sanders and De Haan (2014), which is expected to be released after publication of this paper.

To our knowledge, daily global observations of aerosol height are presently not available on an operational basis. Aerosol profiles are provided regularly by ground-based lidar systems (e.g., EARLINET: European Aerosol Research LIdar NETwork; Pappalardo et al., 2014) or by the spaceborne lidars aboard the Cloud-Aerosol Lidar and Infrared Pathfinder Satellite Observation (CALIPSO) satellite and the future Earth Clouds, Aerosols and Radiation Explorer mission (EarthCARE; Illingworth et al., 2014). These active sensors have a high vertical resolution but they only observe at specific locations or in narrow tracks. We also mention the stereoscopic plume height retrievals from the Multi-angle Imaging SpectroRadiometer (MISR), which are, for example, discussed in Kahn et al. (2007), Nelson et al. (2008), and Val Martin et al. (2010). Furthermore, in the work by Dubuisson et al. (2009), a method is presented to retrieve the height of dust plumes over the ocean using reflectances in the two O_2 A band channels from the multispectral MERIS and POLarization and Directionality of the Earth's Reflectance (POLDER) imagers. In this method, aerosol optical thickness is retrieved in a separate step first and used as an input for the actual plume height retrieval. Finally, we mention reports of existing operational cloud retrievals observing exceptionally optically thick aerosol plumes (Wang et al., 2012; Dirksen et al., 2009).

This paper is structured as follows. Section 2 presents a simulation study discussing the role of the surface albedo in retrieval of aerosol height from the O_2 A band. Section 3 provides a more detailed sensitivity study investigating the effect of model errors in assumed aerosol optical properties for aerosols typically occurring in the free troposphere. Section 4 summarises GOME-2A instrument characteristics relevant for this paper. Section 5 discusses the selection and cloud-clearing of aerosol scenes that are used as an input for the GOME-2A retrieval experiments. In this paper, a scene corresponds to a 3-minute orbit granule. Section 6 describes the retrieval setup (forward model and inversion step). Section 7 presents results of GOME-2A scene retrievals for two

experimental baseline conditions (one in which the surface albedo is retrieved and one in which it is not). Section 8 illustrates a number of algorithm sensitivities by presenting further retrieval experiments using a subset of 16 GOME-2A pixels (called target pixels). In Sect. 9, retrieved aerosol layer heights for these target pixels are compared against lidar measurements. The lidar measurements are also used in retrieval simulations showing the effect of profile shape on retrieved aerosol layer height. Section 10 describes a simulation study investigating this effect in more detail. A discussion and conclusions are given in Sect. 11.

Throughout this paper, height is used as a general indication of vertical location, which can be expressed in terms of pressure in units of hPa or in terms of altitude (above ground level) in units of km. Finally, we remark that a companion paper (Lelli et al., 2016) in this issue describes a science verification of the Aerosol Layer Height algorithm using observations of an optically thick volcanic ash plume near Iceland in May 2010.

2 Should the surface albedo be a fit parameter?

In this section, we discuss in some detail why in one of the two experimental conditions for the GOME-2A scene retrievals we also fit the surface albedo when retrieving aerosol properties from the O_2 A band. It is difficult to separate effects of the surface albedo and aerosol optical thickness from continuum reflectances, but independent information about the two parameters is available from the spectral shape of the absorption band: in the case of single scattering, photons backscattered by aerosols follow shorter paths through the atmosphere than photons reflected by the surface and they will thus have a smaller chance of being absorbed. Indeed, two different combinations of surface albedo and aerosol optical thickness that give the same continuum reflectance may be distinguished from their reflectance spectra inside the absorption band, as is illustrated in Fig. 1 (left panel). The spectrum plotted in red corresponds to the scenario of an aerosol layer between 700 and 600 hPa (P_{mid} of 650 hPa) with an optical thickness (τ) at 760 nm of 0.3 over a ground surface with albedo (A_{s}) of 0.2. The spectrum plotted in green corresponds to the scenario of an aerosol layer with the same height and pressure thickness but with a different optical thickness and for a surface with a different albedo. The combination of aerosol optical thickness and surface albedo is chosen such that the continuum reflectance remains the same as in the first scenario. Note that the two spectra show differences inside the absorption band. For comparison, the spectrum plotted in blue corresponds to the scenario of an aerosol layer moved to a different height but with optical thickness and surface albedo kept the same as in the first scenario. This spectrum differs from the first two also inside the absorption band. Spectra are calculated for TROPOMI's resolution in the near-infrared band of 0.38 nm (anticipated at the time of writing). Also illustrated in Fig. 1 (right panel) are derivatives with respect to aerosol layer mid pressure (P_{mid}), aerosol optical thickness (τ) and surface albedo (A_{s}) for the example scenario. We cannot simultaneously fit surface albedo and aerosol optical thickness when the spectral shape of the derivatives is the same. The question of whether derivatives for a particular scenario are eventually sufficiently different has to be answered by actually doing the (non-linear) retrieval and by subsequently performing an error analysis.

Of course, in order to simplify the retrieval problem one may ask whether it is possible to retrieve aerosol properties while fixing the surface albedo at values provided by climatologies. We have done retrieval simulations investigating the effect on retrieved aerosol properties of uncertainties typically associated with surface albedo climatologies. Figure 2 shows representative results for an aerosol layer over land (the example scenario mentioned above). We assume the climatological (a priori) 1σ error to be 0.02 for land surfaces. The forward model and inversion scheme are the same as used in the GOME-2A retrievals (described in detail in Sect. 6), except for the instrument model (here TROPOMI spectral response function and noise model). Also, for simplicity we take the surface albedo to be independent of wavelength. The left panel shows biases in retrieved aerosol layer pressure when the true surface albedo deviates from the value assumed in retrieval ("climatology"). The three plot lines correspond to retrievals in which the surface albedo is not fitted (a priori error of 0.0), the surface albedo is fitted with an a priori error equal to the climatological error, and the surface albedo is fitted when unconstrained by a priori information (large a priori error of 0.2). When the surface albedo is fixed in the retrieval, small deviations of the true surface albedo cause pressure biases well above 100 hPa and non-convergent retrievals (missing data points). For darker surfaces, the effect is more moderate but still significant. For example, when the true surface albedo is 0.04 but the albedo assumed in retrieval is 0.03, retrieved aerosol layer pressure for the example scenario is almost 100 hPa too high (not shown). The right panel of Fig. 2 illustrates the situation in a different way. In this plot we show precision of retrieved aerosol layer pressure and optical thickness as a function of the a priori error in the surface albedo. The three plot lines of the left panel thus correspond to three distinct points on the x axis of the plot in the right panel. One can see that auxiliary information about the surface albedo should have a 1σ error smaller than about 10^{-3} to 10^{-4} before it starts constraining the retrieval of aerosol properties, which is a very small number. In other words, the O_2 A band contains independent information about the surface albedo and aerosol optical thickness. Of course, this information is more pronounced the more elevated aerosols are (i.e., the larger the pressure difference between the aerosols and the surface is).

Thus, when the surface albedo is fixed, aerosol height retrieved from the O_2 A band will be biased, or the retrieval will not converge for typical uncertainties in surface

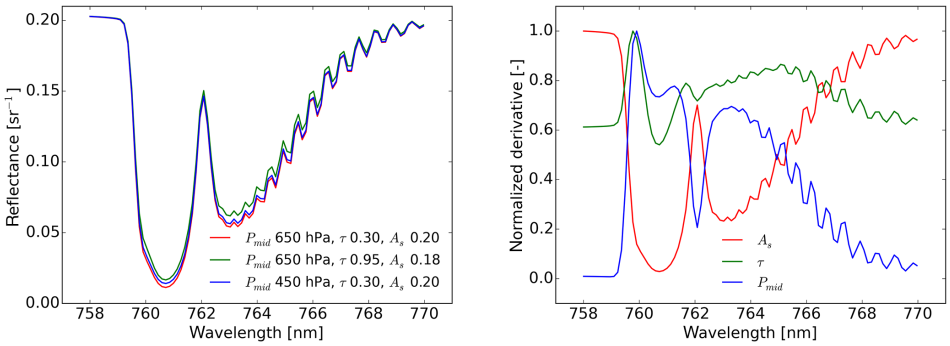

Figure 1. Left panel: simulated top-of-atmosphere reflectance spectra for three different aerosol scenarios at a resolution of 0.38 nm. The solar zenith angle is 50° and the viewing direction is nadir. The spectrum plotted in red corresponds to the example scenario of an aerosol layer between 700 and 600 hPa with an optical thickness at 760 nm of 0.3 over a ground surface with albedo of 0.2. The spectrum plotted in green corresponds to the scenario of an aerosol layer with the same height and pressure thickness but with a different optical thickness and for a surface with a different albedo such that the continuum reflectance remains the same. For comparison, the spectrum plotted in blue corresponds to the scenario of an aerosol layer moved to a different height but with optical thickness and surface albedo the same as in the example scenario. Signal-to-noise ratios for these reflectance levels expected for TROPOMI are about 1000 in the continuum to about 250 in the deepest part of the absorption band. Right panel: derivatives of reflectance with respect to surface albedo, aerosol optical thickness and aerosol layer mid pressure for the example aerosol scenario. Derivatives are normalised to 1.0 at their respective maximums. Both panels: the aerosol has a single scattering albedo of 0.95 and a Henyey–Greenstein phase function with an asymmetry parameter of 0.7. The forward model for these calculations is the same as the forward model used in the GOME-2A retrievals. For simplicity, we assume the surface albedo to be independent of wavelength. Furthermore, the temperature profile corresponds to a mid-latitude summer atmosphere and the surface pressure is 1013 hPa.

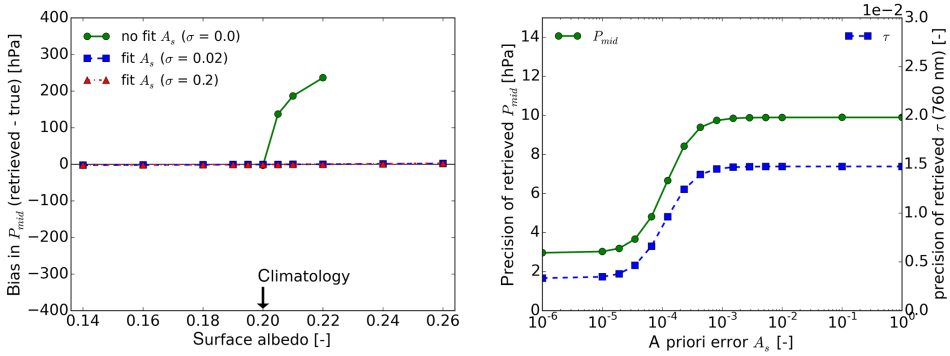

Figure 2. Left panel: results of retrieval simulations showing the bias in retrieved aerosol layer mid pressure as a function of the true surface albedo for three different a priori errors. The a priori value for the surface albedo is 0.20 ("climatology"). Results are shown for the example aerosol scenario (aerosol layer between 700 and 600 hPa with optical thickness at 760 nm of 0.3, surface albedo of 0.2). Missing data points indicate non-converging retrievals. Right panel: results of retrieval simulations showing precision of retrieved aerosol layer mid pressure and optical thickness as a function of the a priori error in the surface albedo. Both panels: a TROPOMI noise model is used which assumes shot noise throughout and a signal-to-noise ratio of 500 at 758 nm for a reference radiance of 4.5×10^{12} photons s^{-1} cm^{-2} sr^{-1} nm^{-1}. The a priori error for aerosol layer mid pressure is 500 hPa and for aerosol optical thickness is 1.0. Other details are the same as in Fig. 1.

albedo climatologies. This is the first reason why we include an experimental condition for the GOME-2A scene retrievals in which the surface albedo is fitted. The second reason to do so is explained in the following. Retrieval of aerosol pressure and optical thickness from the O_2 A band requires of course an assumed aerosol model, but often accurate a priori information about the aerosol optical properties is lacking. As discussed above, the target parameter of the TROPOMI O_2 A band Aerosol Layer Height product is, however, aerosol pressure. In retrieval simulations we have observed that this parameter becomes quite insensitive to the assumed aerosol model if we simultaneously fit the surface albedo (see Sanders and De Haan, 2013). This is illustrated for the example scenario in Fig. 3. We investigate the bias in retrieved aerosol layer pressure as a function of a model error in the single scattering albedo. The value assumed in retrieval is 0.95 ("model value"). This time we show results for a sea surface (left panel) and a land sur-

face (right panel). One can see that in the case of a model error in the single scattering albedo, aerosol layer pressure is biased significantly and retrievals do not converge when the surface albedo is fixed in retrieval. Aerosol optical thickness and the surface albedo are biased as well (not shown). This effect is more moderate for the darker surface. For example, if the true single scattering albedo is 1.0 while the assumed value is 0.95, retrieved aerosol pressure is too high by about 20 hPa for aerosols over sea and by about 180 hPa for aerosols over land. Biases in retrieved aerosol layer pressures and non-convergences almost disappear when the surface albedo is included in the fit. Aerosol optical thickness and surface albedo, however, remain biased (not shown) and as a consequence retrieved values depend on the particular aerosol model assumed in retrieval (one might call them effective quantities). Since aerosol height is the target parameter, this finding is an important reason why at this stage of algorithm development we do not put effort in defining the most realistic aerosol model for every aerosol scene. Instead, in all retrievals presented in this paper we simply model the aerosol with a single scattering albedo of 0.95 and a Henyey–Greenstein phase function with asymmetry parameter of 0.7.

As an important caveat, we mention that correlations between errors in fit parameters for an O_2 A band aerosol retrieval are typically very high. Absolute values of correlation coefficients (r) are often well above 0.9 and can sometimes become as high as 0.999. As an example, Table 2 lists correlation coefficients for retrieval of the example aerosol layer over land and over sea. The corresponding a posteriori errors, however, are small, as was shown in the right panel of Fig. 2. Apparently, parameters can be fitted with small precision errors in the case that errors are indeed so highly correlated. Derivatives of reflectance with respect to the various fit parameters are similar, yet there are small but significant differences (see right panel of Fig. 1), which cause correlation coefficients to be smaller than one and make it possible to simultaneously fit parameters. Still, we should anticipate retrieval becoming sensitive to the many other systematic and quasi-random model and instrument errors present in real data when moving from the retrieval simulations reported in this section to the GOME-2A retrievals reported in the next sections. Finally, we remark that we are not aware of previous studies on O_2 A band cloud or aerosol retrieval reporting a posteriori correlation coefficients.

Table 2. A posteriori correlation coefficients (r) for a simulated retrieval of an aerosol layer between 700 and 600 hPa with optical thickness at 760 nm of 0.3 located over land and over sea. Either mid pressure and optical thickness or mid pressure, optical thickness and surface albedo are fitted. Other details are the same as in Figs. 1 and 2.

Correlation coefficient (r)	$P_{\mathrm{mid}} - \tau$	$P_{\mathrm{mid}} - A_{\mathrm{S}}$	$\tau - A_{\mathrm{S}}$
land/fit P_{mid}, τ, A_{S}	−0.992	0.957	−0.975
sea/fit P_{mid}, τ, A_{S}	−0.989	0.985	−0.999
land/fit P_{mid}, τ	−0.917	–	–
sea/fit P_{mid}, τ	−0.612	–	–

3 Sensitivity of retrieved aerosol layer height and optical thickness to the aerosol optical properties

As explained in the previous section, we apply a single aerosol model to the various GOME-2A scenes investigated in this study. From the perspective of operational processing, it is perhaps convenient to use a single aerosol model globally when the inaccuracy introduced in retrieved aerosol height is limited. But of course, we may optimise the assumed aerosol model or even implement a sophisticated model selection scheme at a later stage of algorithm development. We are not arguing against proceeding in that way here. In this section we discuss a more detailed sensitivity study investigating the effect of errors in the assumed aerosol model on retrieved aerosol layer height and aerosol optical thickness. We focus on desert dust, carbonaceous aerosols and volcanic ash, which are the dominant aerosol types in the free troposphere. When they occur, these aerosols typically have relatively high optical thicknesses.

The desert dust model and the carbonaceous aerosol model are taken from the aerosol project of ESA's Climate Change Initiative (CCI) program and they are described in De Leeuw et al. (2015). The coarse mode dust model is based on T-matrix calculations and the carbonaceous aerosol model is the fine mode strongly absorbing aerosol model based on Mie calculations. Finally, the volcanic ash model is based on the synthetic average volcanic aerosol model from the Amsterdam–Granada Light Scattering Database (Muñoz et al., 2012). The phase function for this model is the average of measured phase functions for nine different volcanic ash samples (Muñoz et al., 2002, 2004; Volten et al., 2001). We calculated the extinction and scattering cross sections again from Mie theory using the average of the measured size distributions as reported by the Amsterdam–Granada database and a complex refractive index calculated from in situ measurements during the 2010 Eyja eruption as reported by Schumann et al. (2011; case "medium"). Extinction and scattering cross sections for the volcanic ash model are calculated at 630 nm, and we assume the same values at wavelengths of the O_2 A band. Table 3 gives values for the extinction cross section and single scattering albedo at 760 nm and other properties. Note that the carbonaceous aerosol and the volcanic ash have similar and relatively low single scattering albedos.

The three aerosol models are used to simulate measurements and a retrieval is subsequently attempted assuming again the default aerosol model. The aerosol layer is between 700 and 600 hPa with varying optical thickness. Settings are the same as in the simulation study of the previous section.

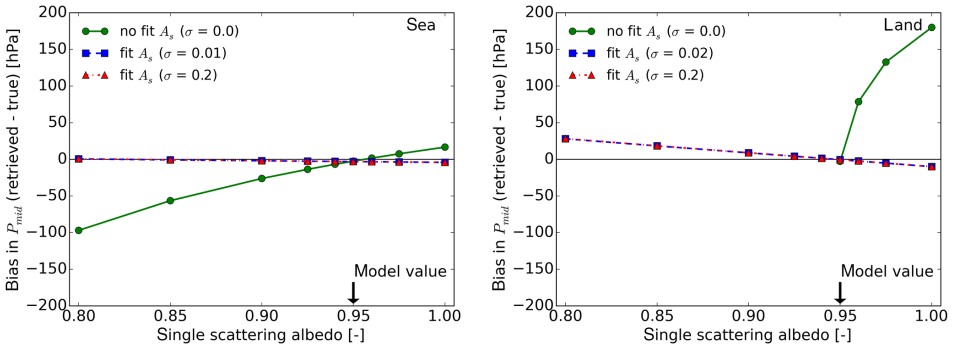

Figure 3. Results of retrieval simulations showing the bias in retrieved aerosol layer mid pressure as a function of the true single scattering albedo for three different a priori errors in the surface albedo. The single scattering albedo assumed in retrieval is 0.95 ("model value"). The aerosol layer is over sea (albedo of 0.03, left panel) or over land (albedo of 0.2, right panel). Missing data points indicate non-converging retrievals. Other details are the same as in Figs. 1 and 2.

Table 3. Summary of aerosol models used in the sensitivity study of Sect. 3. The table lists the extinction cross section (C_{ext}), single scattering albedo (ω) and asymmetry parameter (g) at 760 nm, and the ratio of the extinction cross section at 760 nm to the extinction cross section at the reference wavelength. The reference wavelength is 550 nm for the carbonaceous aerosol and desert dust model and 630 nm for the volcanic ash model.

Aerosol model	$C_{\text{ext}}^{760\,\text{nm}}$ [μm^{-2}]	$\omega^{760\,\text{nm}}$ [–]	$g^{760\,\text{nm}}$ [–]	$C_{\text{ext}}^{760\,\text{nm}}/C_{\text{ext}}^{\text{ref}}$ [–]
Carbonaceous aerosol	1.8×10^{-2}	0.76	0.57	0.57
Desert dust	$1.1 \times 10^{+1}$	0.97	0.71	1.0
Volcanic ash	1.6×10^{-1}	0.76	0.65	1.0

Figure 4 shows the bias in retrieved aerosol layer mid pressure and retrieved aerosol optical thickness as a function of the true optical thickness. Biases in aerosol layer pressure are moderate for retrieval over sea. In the case of the dust aerosol, which absorbs only little in the near-infrared range, this is true even when the surface albedo is not fitted. For land, biases become larger or retrieval does not converge (missing data points). Fitting the surface albedo helps to ameliorate biases and improve convergence. These observations confirm what has already been concluded in the previous section. Furthermore, we see that for specific ranges of the optical thickness larger retrieval biases occur or biases become variable (see, for example, retrieval for the carbonaceous aerosol between 0.1 and 0.2 optical thickness). The range in which retrieval becomes singular depends on the particular combination of aerosol optical thickness, aerosol height, aerosol optical properties (notably the phase function), the surface albedo and the observation geometry and is therefore hard to predict. This has been noted before in Sanders and De Haan (2013). Such a singularity can also occur at higher aerosol optical thickness (see Sanders and De Haan, 2014). Comparing biases against the threshold requirement of 100 hPa, we see that biases are acceptable for optical thicknesses larger than about 0.2. With respect to non-converging retrievals, we remark that convergence can be improved by, for example, decreasing the signal-to-noise ratio, as we do in the GOME-2A retrievals presented below. The measurement error covariance matrix in the retrieval simulations shown here is only filled with nominal noise errors, which may be too tight for convergence when also calibration errors or other systematic errors are present.

We mention that more extensive retrieval simulations investigating the effects discussed above and many other retrieval sensitivities are presented in Sanders and De Haan (2014). In this paper, we present a number of sensitivity experiments using GOME-2A spectra, rather than simulated spectra, to further investigate the retrieval. In conclusion, from simulation studies we learn that the surface albedo should be a fit parameter when retrieving aerosol properties from the O_2 A band. In the following sections we investigate whether this conclusion also holds for retrievals with real spectra.

4 GOME-2 instrument characteristics

The GOME-2 instruments are in polar orbits with local equator crossing times of about 9.30 h (descending node). In this paper, we only consider observations by GOME-2 on Metop-A (GOME-2A). The swath of GOME-2A had been 1920 km until mid July 2013 at which point it was reduced by a factor of 2. In nadir scanning mode, the scanning mirror has a return time of 6 s, taking 4.5 s for the forward scan (east to west) and 1.5 s for the backward scan (west to east). In this work,

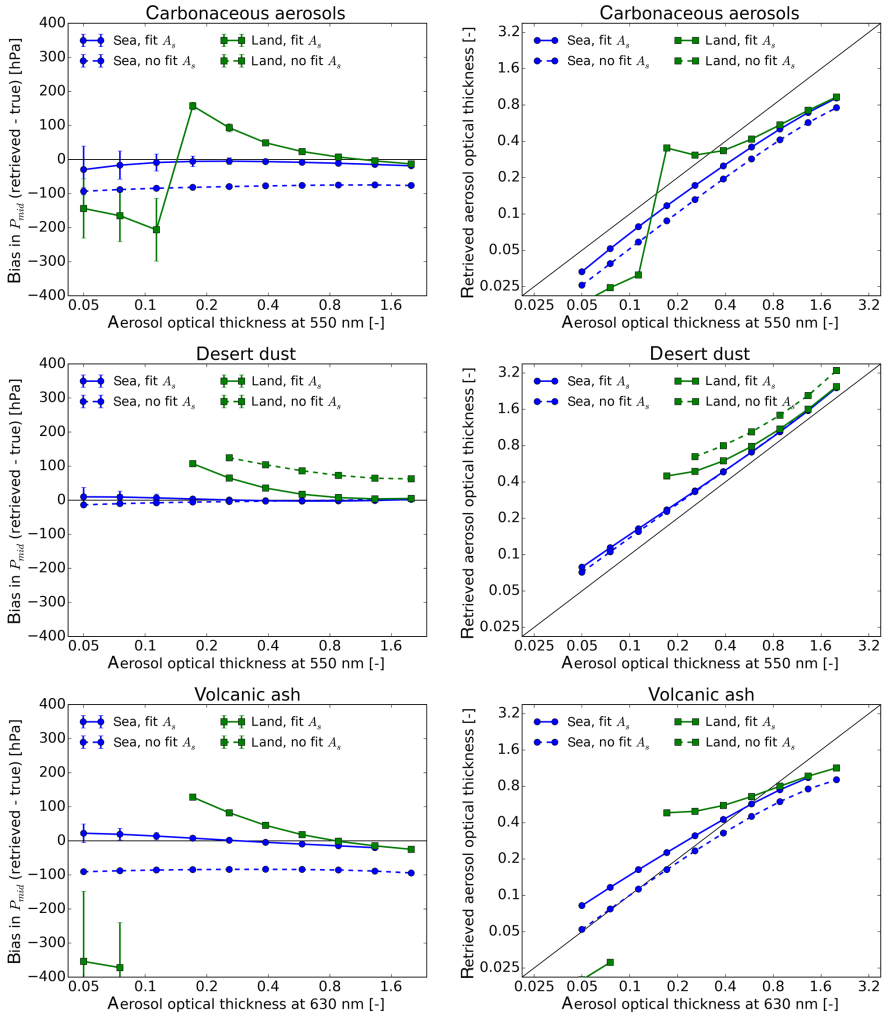

Figure 4. Results of retrieval simulations showing the bias in retrieved aerosol layer mid pressure (left column) and retrieved aerosol optical thickness (right column) as a function of the true aerosol optical thickness for three different aerosol types (rows). Measurements are simulated for a carbonaceous aerosol (top row), a desert dust (middle row) and a volcanic ash type (bottom row), while in the retrieval the default aerosol model is assumed (single scattering albedo of 0.95 and a Henyey–Greenstein phase function with asymmetry parameter of 0.7). The four plot lines correspond to sea (blue, circles) and land (green, squares) and to not fitting (dashed lines) and fitting (solid lines) the surface albedo. The aerosol layer is located between 700 and 600 hPa. Missing data points indicate non-converging retrievals. The solar zenith angle is 50° and the viewing direction is nadir. All other settings are the same as in the simulation study of Sect. 2 (see also Figs. 1 and 2).

only forward pixels are considered. The scan speed profile is such that the across track pixel size is approximately constant. The across track pixel size is mainly determined by the integration time, which generally is 0.1875 s for spectrometer Band 4 for the sunlit part of the orbit track. Thus, the across track forward pixel size is 80 km for the nominal 1920 km swath and 40 km in reduced swath mode (aerosol scene 06 in this work). The along track pixel size at nadir is 40 km and is primarily determined by the instrument's along track instantaneous field of view. Band 4 runs from 584 to 798 nm and has a spectral sampling of about 0.21 nm. The instrument spectral response function in Band 4 has a full width at half maximum (FWHM) of approximately 0.53 nm, which is coarser than TROPOMI's resolution (FWHM of 0.38 nm). Finally, we mention that GOME-2 has so-called polarisation measurement devices (PMDs), which measure P-polarised and S-polarised light in a number of wavelength bands. These measurements are used to correct radiance spectra for the instrument's polarisation sensitivity. They can also provide sub-pixel information for spectrometer measurements, because PMD ground pixels are eight times smaller in the across track direction (e.g., 10 by 40 km for a spectrometer ground pixel of 80 by 40 km). More information can be found in EUMETSAT (2014a). Without further clarification, the GOME-2A ground pixel refers to the ground pixel of the spectrometer throughout this paper.

5 Selection of aerosol scenes and masking of clouds

We first compiled a list of 16 aerosol scenes that served as an input for the GOME-2A retrieval experiments. In this paper, we define a scene as a 3-minute granule of GOME-2A observations, which covers an area of about 1920 km across track by 1200 km along track (at nadir) for ground pixel sizes of 80 by 40 km (at nadir). Scenes were selected not only for the presence of aerosols but also for the availability of lidar measurements within the scene. We initially focussed on ground-based measurements because we might find good spatiotemporal collocation with the GOME-2A overpass for these lidar measurements. Ground-based measurements from the Cabauw Experimental Site for Atmospheric Research (CESAR) and the EARLINET station at Cabauw (Netherlands), from EARLINET stations at Evora (Portugal) and Granada (Spain), and from the Micro Pulse Lidar NETwork (MPLNET) station at Santa Cruz (Canary Islands) are included in this study. We also used airborne measurements taken aboard the Facility for Airborne Atmospheric Measurements's (FAAM) Atmospheric Research Aircraft during two dedicated campaigns over the North Sea (Eyjafjallajökull eruption) and the Aegean Sea (the European Space Agency's CARBONEXP campaign). Finally, we took satellite-based lidar measurements from CALIPSO into account. The initial checking of the presence of significant amounts of aerosols and of cloud conditions was done using AERONET aerosol optical thickness plots, lidar quicklooks and RGB images from the MODerate resolution Imaging Spectroradiometer (MODIS). Table 4 provides a short description of the 16 aerosol scenes that were eventually selected.

Having lidar measurements available within the geographical area of the aerosol scene that are also reasonably close in time to the GOME-2A overpass is a severe constraint, because of the sparse spatiotemporal sampling of lidar measurements. For example, exceptionally thick ash plumes close to an erupting volcano, which may have been an easy starting point for our case studies, were not included as there are no such aerosol cases (to our knowledge) for which there are nearby lidar measurements. As a consequence, the aerosol scenes have aerosol optical thicknesses that are moderate (see Table 4).

GOME-2A aerosol scenes were cloud-cleared using four conventional AVHRR threshold tests (EUMETSAT, 2011). These tests are (i) a brightness temperature test in the 11 µm channel to detect medium to high clouds, (ii) a brightness temperature difference test for the 11 and 12 µm channels to detect thin cirrus clouds, (iii) an albedo test using the two visual channels (one for land, the other for sea) to detect bright low clouds, and (iv) a spatial coherence test for the 11 µm channel to detect broken clouds over sea. For every AVHRR pixel, if one of the tests indicated the presence of a cloud, the AVHRR pixel was considered cloudy. Then, a cloud fraction for the GOME-2A ground pixel was derived by dividing the number of cloudy AVHRR pixels by the total number of AVHRR pixels falling within the spectrometer's footprint. Aerosol height retrievals in this paper are only attempted for GOME-2A pixels with zero AVHRR cloud fraction. Table 4 lists the number of cloud-free pixels for every aerosol scene.

We mention here that we did not take AVHRR cloud information directly from the AVHRR level-1b product but used EUMETSAT's (European Organisation for the Exploitation of Meteorological Satellites) new Polar Multi-sensor Aerosol Properties product (PMAp) instead (EUMETSAT, 2014b). This product provides spectral aerosol optical thickness derived from GOME-2's PMD broadband radiances. As a support field, PMAp also provides an AVHRR cloud fraction for PMD ground pixels using the approach described above. AVHRR pixels are accurately collocated to PMD ground pixels (EUMETSAT, 2014b). We used cloud fractions for PMD ground pixels to calculate cloud fractions for spectrometer ground pixels.

Finally, we also selected a target GOME-2A pixel for every scene resulting in a set of 16 pixels. This set serves two purposes: first, it is used in extensive retrieval experiments investigating a number of retrieval sensitivities and second, it is used for comparison against lidar measurements. Sensitivity experiments are limited to a set of 16 target pixels because computation time currently renders difficult investigating sensitivities for entire aerosol scenes. Target pixels were carefully selected according to the following criteria: (i) spatiotemporal collocation with lidar measurement, (ii) cloud-free conditions (AVHRR cloud mask), (iii) high aerosol optical thickness (Absorbing Aerosol Index; PMAp aerosol optical thickness; MODIS Terra aerosol optical thickness), (iv) homogeneous pixel (no coastal pixel, low variability of surface elevation inside pixel); and (v) outside sun glint region (threshold of 18° on sun glint angle, i.e., the angle between viewing direction and direction of specular reflection). These criteria could not be fulfilled all at the same time, and a qualitative trade-off had to be made. An overview of the 16 target pixels is shown in Fig. 5 (the numbering of the target pixels corresponds to the numbering of the scenes in Table 4).

Also shown in Fig. 5 are the locations of the corresponding lidar measurements. Often, the lidar profile showed cloud-free conditions while the AVHRR cloud mask unfortunately indicated the significant presence of clouds for the overlapping GOME-2A pixel. The high chance of cloud contamination due to the large GOME-2A ground pixel size is one of the reasons why good spatial collocation with the lidar measurement was not achieved for every target pixel. Sometimes, there was also a significant time difference between the lidar measurement and the GOME-2A observation (e.g., in the case of a Raman lidar measurement in the early evening). For several cases, two lidar measurements were included in the analysis. Table 5 gives a description of each lidar measurement and lists the spatiotemporal distance to the target pixel.

We emphasise here that we are not attempting a comprehensive lidar validation of our results in this study but only

Table 4. Description of the 16 aerosol scenes used in the GOME-2A retrieval experiments. Here, an aerosol scene is a 3-minute granule of GOME-2A observations, which consists of 720 pixels in total.

Scene	Date	Scene description: geographical location; surface type; aerosol type and vertical distribution	Mean/maximum MODIS Terra aerosol optical thickness [4]	Maximum Absorbing Aerosol Index (AAI)	Number of cloud-free GOME-2A pixels (out of 720) [5]
01	3 Sep 2011	Eastern Mediterranean region; land and sea; (polluted) dust up to about 5 km	0.29/0.90	2.3	135
02	6 Sep 2011	Eastern Mediterranean region; land and sea; polluted dust up to about 3 km	0.21/0.63	2.7	136
03	20 Apr 2011	Northwest Europe; land and sea; continental pollution, mainly in boundary layer	0.28/2.07	1.2	109
04	9 Jul 2013	Northwest Europe; land and sea; elevated smoke transported across the Atlantic from forest fires in North America, continental pollution in boundary layer	0.21/0.64	1.5	167
05	2 Jul 2009	Northwest Europe; land and sea; continental pollution, multi-layered, up to about 2 km	0.24/0.82	1.4	87
06 [1]	18 Jul 2013	Northwest Europe; land and sea; continental pollution, multi-layered, can extend up to 5 km	0.16/0.53	1.0	73
07	12 May 2011	Northwest Africa; land and sea; Saharan dust outbreak, elevated dust layers up to 5 km	0.63/1.34	5.0	27
08	31 Jul 2011	Atlantic Ocean off the coast of Northwest Africa; sea; Saharan dust outbreak, elevated dust layers up to 6 km	0.33/1.75	3.1	17
09	10 Aug 2011	Atlantic Ocean off the coast of Northwest Africa; sea; Saharan dust outbreak, elevated dust layers up to about 5 km	0.58/1.27	3.4	54
10	28 Jun 2012	Atlantic Ocean off the coast of Northwest Africa; sea; Saharan dust outbreak, elevated dust layers up to 6 km	0.18/1.20	3.8	53
11	28 Jun 2012	Western Mediterranean region; land and sea; Saharan dust transported to Southern Europe, dust layer up to 5 km	0.54/1.55	4.2	126
12	7 Apr 2011	Western Mediterranean region; land and sea; Saharan dust transported to Southern Europe, dust up to 5 km, sometimes also continental pollution in boundary layer	0.12/0.82	3.5	226
13 [2]	7 Apr 2011	Atlantic Ocean west of Gibraltar; mainly sea; Saharan dust transported to Southern Europe, dust up to 5 km	0.58/3.25	4.2	89
14	18 Apr 2010	Northwest Europe; land and sea; volcanic ash from the Eyjafjallajökull eruption, dense plume passes over Cabauw at about 2 km around noon that day	0.18/0.78	2.4	184
15	19 May 2010	Northwest Europe; land and sea; volcanic ash from the Eyjafjallajökull eruption, geometrically thin layer around 2 km is present over Cabauw	0.19/0.65	2.1	4
16 [3]	17 May 2010	Northwest Europe; land and sea; volcanic ash from the Eyjafjallajökull eruption, plume over the North Sea between about 4 and 6 km	0.28/0.93	2.4	6

[1] Reduced swath for GOME-2 on Metop-A: ground pixels are 40 km by 40 km.
[2] This dust outbreak is described in detail in Preißler et al. (2011).
[3] The flight of the FAAM aircraft and measurements taken aboard are described in Johnson et al. (2012).
[4] Mean and maximum of MODIS Terra aerosol optical thicknesses (at 550 nm) for MODIS ground pixels collocated with GOME-2A pixels in the scene. MODIS aerosol optical thicknesses are from Dark Target Land and Ocean algorithms. Note that the Terra platform lags Metop-A by about 1 hour.
[5] For a description of the cloud mask applied to the GOME-2A spectrometer pixels, see main text.

do a first comparison. A validation is beyond the scope of this paper, and given the present GOME-2A retrieval results it is not needed for our purposes at this point (to be discussed in detail in Sect. 9). We will primarily use lidar measurements to better understand the difference in retrieval outcome when the surface albedo is retrieved simultaneously with aerosol parameters or when it is fixed in the retrieval.

Table 5. Description of the lidar measurements that are used in the comparison with retrieved aerosol heights for GOME-2A target pixels. Spatial distance is the distance between the centre of the GOME-2A target pixel and the location of the lidar measurement. Recall that GOME-2A pixels are usually 80 km by 40 km. Temporal distance is defined as the time of the lidar measurement minus the observation time for the GOME-2A target pixel. Reported lidar extinction profiles are not instantaneous but averaged over a certain time window. Averaging times vary with lidar systems and atmospheric conditions.

Scene	Lidar description	Spatial distance to target pixel [km]	Temporal distance to target pixel [hh:mm]	Remarks
01	FAAM aircraft; extinction at 355 nm	81 km	+01:14	Assumed lidar ratio 65 sr
02	CALIPSO; extinction at 532 nm	102 km	about +02:35	CALIPSO level-2
03	Cabauw/CESAR; extinction at 355 nm	46 km	00:00	Assumed lidar ratio 50 sr
04	Cabauw/EARLINET; extinction at 355 nm	148 km	about +01:45	Raman lidar measurement
	CALIPSO; extinction 532 nm	140 km	about +02:43	CALIPSO level-2
05	CALIPSO; extinction 532 nm	14 km	about +02:50	CALIPSO level-2
	Cabauw/EARLINET; extinction at 355 nm	429 km	about −01:37	Raman lidar measurement
06	CALIPSO; extinction 532 nm	55 km	about +02:24	CALIPSO level-2
	Cabauw/EARLINET; extinction at 355 nm	504 km	+01:31	Assumed lidar ratio 50 sr
07	CALIPSO; extinction 532 nm	43 km	about +03:27	CALIPSO level-2
	Santa Cruz/MPLNET; extinction at 532 nm	540 km	about −00:15	Assumed lidar ratio 50 sr
08	Santa Cruz/MPLNET; extinction at 532 nm	244 km	about −02:02	Assumed lidar ratio 50 sr
09	Santa Cruz/MPLNET; extinction at 532 nm	106 km	about +00:06	Assumed lidar ratio 50 sr
10	CALIPSO; extinction 532 nm	8 km	about +03:34	CALIPSO level-2
	Santa Cruz/MPLNET; extinction at 532 nm	1143 km	about +00:16	Assumed lidar ratio 50 sr
11	CALIPSO; extinction 532 nm	145 km	about +03:42	CALIPSO level-2
	Granada/EARLINET; extinction at 355 nm	47 km	about +10:00	Raman lidar measurement
12	Granada/EARLINET; extinction at 532 nm	101 km	+00:02	Assumed lidar ratio 50 sr
13	Evora/EARLINET; extinction at 355 nm	4 km	about −07:07	Raman lidar measurement
	CALIPSO; extinction 532 nm	142 km	about +02:36	CALIPSO level-2
14	Cabauw/CESAR; extinction at 355 nm	76 km	+00:01	Assumed lidar ratio 50 sr
15	Cabauw/CESAR; extinction at 355 nm	168 km	+01:39	Assumed lidar ratio 50 sr
16	FAAM aircraft/extinction at 355 nm	318 km	+04:54	Assumed lidar ratio 65 sr

6 Description of the retrieval setup

Here, we summarize main aspects of the forward model and the inversion scheme and describe the implementation for retrievals with GOME-2A as presented in this paper. The forward model and related modules are part of a software package developed at the Royal Netherlands Meteorological Institute (KNMI) called DISAMAR. The abbreviation DISAMAR stands for Determining Instrument Specifications and Analyzing Methods for Atmospheric Retrieval.

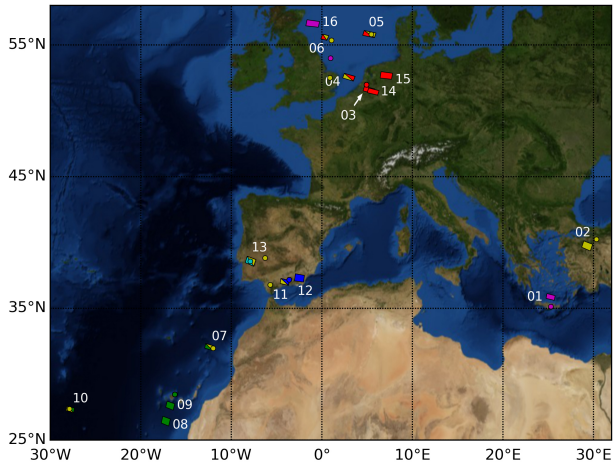

Figure 5. Overview of GOME-2A target pixels (numbered quadrangles) and corresponding lidar measurements (circles). The lidar measurements are described in Table 5. Color code for lidar measurements: FAAM aircraft (magenta), CALIPSO (yellow), Cabauw (red), Santa Cruz (green), Granada (blue), and Evora (cyan). For some pixels, two lidar measurements are available for evaluation. There are nine GOME-2A target pixels over sea (target pixels 01, 04, 05, 06, 07, 08, 09, 10, 16) and seven over land (target pixels 02, 03, 11, 12, 13, 14, 15). The aerosol scenes are described in Table 4.

6.1 Forward model

Monochromatic reflectances in the O_2 A band are calculated online using the doubling-adding method (e.g., De Haan et al., 1987; Hovenier et al., 2004). Multiple scattering is included in the calculations, but polarisation and rotational Raman scattering are ignored. An efficient high-resolution wavelength grid is constructed by defining small wavelength intervals bounded by strong O_2 line positions and using Gaussian division points for each interval. This results in about 3000 line-by-line calculations for a fit window extending from 758 to 770 nm and an oxygen absorption cross section that includes the three major isotopologues. The atmosphere is divided into 24 homogeneous layers, the distribution of which is not equidistant but again follows a Gaussian integration scheme. Finally, 9 Gaussian points (18 streams) are used for integration over the polar angle. Derivatives are calculated in a semi-analytical manner using reciprocity (equivalent to the adjoint method, e.g., Landgraf et al., 2001).

In addition to line absorption by O_2, first-order line mixing and collision-induced absorption by O_2-O_2 and O_2-N_2 are included in the oxygen absorption cross section according to Tran et al. (2006) and Tran and Hartmann (2008). Line parameters for the three major isotopologues are taken from the Jet Propulsion Laboratory database in agreement with Tran and Hartmann (2008). In the baseline retrieval setup, the resulting absorption cross section is multiplied by 1.03 following Butz et al. (2013) and Crisp et al. (2012).

Temperature profiles and surface pressures were taken from the European Centre for Medium-range Weather Forecasts' (ECMWF) Interim reanalysis fields. Reanalysis data are available every 6 h (model times: 00:00, 06:00, 12:00, and 18:00 UTC) with a native spatial resolution of about 80 km. We used data on a 0.5° by 0.5° regular latitude–longitude grid. Note that this resolution is comparable to the size of the GOME-2 pixel. In the spatial dimension we took meteorological data for the model grid point closest to the center coordinate of the GOME-2A pixel. In the temporal dimension, we used linear interpolation between the two closest model times to determine meteorological parameters at the time of the GOME-2A observation.

Next to oxygen absorption and Rayleigh scattering, scattering and absorption by aerosols takes place in the atmosphere. In the baseline retrieval setup, we assume a single aerosol layer that is modelled as a layer of particles with a constant particle volume extinction coefficient and particle single scattering albedo. Also the pressure thickness is assumed constant and taken to be 50 hPa in all GOME-2A retrievals. By default, aerosols have a single scattering albedo of 0.95 and a Henyey–Greenstein phase function with asymmetry parameter of 0.7. There is no particular reason for choosing these values of single scattering albedo and asymmetry parameter other than that they are intermediate to values typically observed (Dubovik et al., 2002). In a similar fashion, we choose a phase function that is smooth and can serve as an approximate phase function for many aerosol types.

The ground surface is modelled as a Lambertian surface, and we allow the surface albedo to depend linearly on wavelength. Albedo values at two wavelength nodes located at the end points of the fit window (758 and 770 nm) are specified and intermediate values are determined by interpolation. A priori values for the albedo at the two nodes are taken from the MERIS black-sky albedo climatology (Popp et al., 2011). Note that for sea pixels this climatology is filled with values from the GOME Lambertian-equivalent reflectivity climatology (Koelemeijer et al., 2003). In one of the sensitivity experiments of Sect. 8, we investigate the effect of fitting fluorescence emissions. Chlorophyll fluorescence from terrestrial vegetation is modeled as an isotropic contribution to the upwelling radiance field at the surface. Also fluorescence emissions are allowed to depend linearly on wavelength and they are specified at the same two wavelength nodes as the surface albedo. We assume fluorescence emissions to be absent a priori.

Finally, we use the measured GOME-2A spectral response functions as described and analysed by Siddans et al. (2007) and the high-resolution solar irradiance spectrum from Chance and Kurucz (2010) to simulate measured reflectance spectra and their derivatives. Instrument stray light can be included in the forward model as a spectrally

smooth (i.e., low-order polynomial in wavelength) additive offset to the simulated measured radiance spectrum. In one of the sensitivity experiments of Sect. 8, we include a spectrally constant stray light offset in the fit and assume the offset to be absent a priori. We specify the additive radiance offset as a percentage of the continuum radiance at 758 nm.

6.2 Inversion

GOME-2A level-1b files provide radiance spectra and a daily irradiance measurement. The product also provides a noise spectrum for each radiance measurement, which we call the nominal noise in this paper. Level-1b files from the latest processor version 5.3 are used.

The atmospheric state vector is determined through a spectral fit of reflectance across the fit window running from 758 to 770 nm and using the Optimal Estimation framework (Rodgers, 2000). The state vector contains in any case aerosol layer mid pressure (P_{mid}) and aerosol optical thickness (τ) at 760 nm. Depending on the experimental condition, the state vector may contain other parameters as well. State vector elements, a priori values and a priori errors are summarised in Table 6. A positive temperature offset means that the entire a priori ECMWF temperature profile is shifted by the offset amount to higher temperatures in the retrieval.

Gauss–Newton iteration is used to find a minimum in the cost function, which is an efficient method if the forward model is only moderately non-linear. However, in the case of non-linear behaviour of the forward model, convergence and the retrieval solution itself may depend on the starting values for the iteration. For example, it has been noted in simulation experiments that the cost function for O_2 A band aerosol retrieval may have multiple local minima (e.g., Fig. 19 in Hollstein et al., 2012; Fig. 6-1 in Sanders and De Haan, 2014). One of the aims of the retrieval experiments reported in this paper is therefore to systematically investigate convergence and stability of the retrieval. For that reason, we now discuss in somewhat more detail the implementation of the Gauss–Newton method in our retrieval setup.

Gauss–Newton iteration is embedded in an iterative scheme with two modifications. First, when the initial state differs strongly from the true state, it is known that the update of the state vector in the case of Gauss–Newton iteration can become very large and lead to a point in state space far from the correct solution. Therefore, if the update of the state vector becomes larger than a pre-defined threshold, we reduce the size of the update. We do this by temporarily decreasing the signal-to-noise ratio of the measurement until the update falls below the threshold. In our GOME-2A retrieval experiments, reduction of the state vector update occurs almost every run, particularly during the first few updates. Second, parameters can attain non-physical values during iteration (e.g., negative optical thickness). For various parameters we have therefore defined boundaries. If a state vector element crosses such a boundary, we simply reset the element to that boundary value. We prefer this method to transformations that make such boundary crossings impossible (e.g., fitting of the logarithm of the optical thickness) because we have experienced that such transformations tend to make the model more non-linear. In our GOME-2A retrieval experiments, we see that boundary resets occur regularly during iteration, also for retrievals that subsequently converge. Examples of boundaries are 0.01 for the minimum aerosol optical thickness and 15 km for the maximum altitude of the aerosol layer.

The maximum allowed number of iterations is 12. Based on results from the GOME-2A retrieval experiments (to be discussed below), we do not expect convergence to significantly improve if this number is increased. An initial round of experiments suggested that convergence does improve significantly if the nominal noise as given in the level-1b product is increased. In these preliminary experiments, we found that multiplying the nominal noise by two improves convergences but does not introduce new retrieval solutions. In all GOME-2A retrieval experiments reported in this paper (the scene retrievals of Sect. 7 as well as the sensitivity experiments of Sect. 8), the nominal noise has therefore first been multiplied by two before a retrieval is attempted.

Finally, convergence and stability of the retrieval is tested by always running the retrieval for a particular GOME-2A pixel in a particular experimental condition multiple times with different initial values. Typically, retrieval is attempted for three initial values for the aerosol layer mid pressure and two initial values for the optical thickness (six runs in total).

7 Results of GOME-2A scene retrievals

Figure 6 shows retrieved aerosol layer mid pressure and aerosol optical thickness for three representative scenes when the surface albedo is not fitted and Fig. 7 shows results for the same scenes when the surface albedo is included in the fit. In both cases also a temperature offset is retrieved. Retrieval is only attempted for cloud-free pixels according to the AVHRR cloud mask described above. Retrievals that did not converge for any of the six attempted runs (i.e., for any of the six different sets of initial values) are represented in white; for retrievals that had at least one convergent run, the solution with the smallest χ^2-value is shown. Quadrangles with red borders indicate pixels that are inside the sun glint region (i.e., sun glint angle smaller than 18°). These pixels are included in the scene retrievals. For every scene, the target pixel, which is used in more extensive sensitivity experiments (Sect. 8) and for which retrieved aerosol layer height is compared against lidar profiles, is indicated with a thick black border. Note that target pixels are always selected outside the sun glint region. Finally, spatial locations of the lidar measurements are indicated with a purple dot.

Out of 1493 cloud-free pixels in total, 842 pixels had at least one converging run when the surface albedo was not

Table 6. State vector elements, a priori values and a priori (1σ) errors. In the default retrieval setup for the GOME-2A scene retrievals (Sect. 7), only the first three or five parameters are fitted. Retrieval is attempted multiple times with different initial values for aerosol layer mid pressure and aerosol optical thickness. Fitting stray light or fluorescence emissions is only done in sensitivity experiments reported in Sect. 8.

Element	A priori value	A priori error
Aerosol layer mid pressure (P_{mid})	[varying]	500 hPa
Aerosol optical thickness (τ) at 760 nm	[varying]	1.0
Temperature offset (ΔT)	0 K	3 K
Surface albedo (A_{s}) at 758 and 770 nm (two nodes)	Climatology	0.2
Stray light (additive radiance offset expressed as a percentage of the continuum radiance at 758 nm)	0 %	3 %
Fluorescence (F_s) at 758 m and 770 nm (two nodes)	0 photons $\mathrm{s}^{-1}\,\mathrm{cm}^{-2}\,\mathrm{sr}^{-1}\,\mathrm{nm}^{-1}$	10^{12} photons $\mathrm{s}^{-1}\,\mathrm{cm}^{-2}\,\mathrm{sr}^{-1}\,\mathrm{nm}^{-1}$

fitted and 1401 pixels had at least one converging run when the surface albedo was fitted. Including the surface albedo in the state vector raised the average number of iterations needed for convergence from 3.9 to 6.5. The average calculation time for one iteration (spectrum and derivatives) is about 30 s on an up-to-date desktop computer. We remark that the computer code is a non-optimised science code.

In agreement with our expectation from the simulation study of Sect. 2, we see poorer convergence when the surface albedo is not fitted. This would then be due to, for example, the model value from the surface albedo climatology being inaccurate. Also inaccuracies in the assumed aerosol model could play a role here. Interestingly, a significant number of pixels still show converging retrievals when the surface albedo is fixed in retrieval. When the surface albedo is fitted, most pixels had at least one converging run. However, in that case we find that retrieved pressures are systematically and significantly lower (i.e., aerosol layer higher in atmosphere), which is unexpected. The systematic differences in retrieved aerosol layer pressure between the two experimental conditions are typically larger than the biases found in the simulation study of Sect. 2. This suggests that other, stronger effects are interfering in the GOME-2A retrievals. Also note that retrieved aerosol layer mid pressures show more realistic values when not fitting the surface albedo than when fitting. Finally, we remark that retrieved parameter values often show an east–west gradient, or rather an interaction with the viewing zenith angle, as well as a land–sea interaction. These interactions could be related to, for example, model errors in the phase function. Such a model error affects retrieved optical thickness and, because of correlated errors, also aerosol pressure.

Figure 8 shows PMAp aerosol optical thickness at 550 nm against retrieved aerosol optical thickness (at 760 nm) for both experimental conditions. PMAp retrieves spectral aerosol optical thickness for PMD ground pixels. The theoretical basis is described in EUMETSAT (2014b) and a first validation with AERONET aerosol optical thickness is reported in EUMETSAT (2014c). Eight PMD ground pixels make up one spectrometer ground pixel. In Fig. 8, the mean of valid PMD subpixel PMAp aerosol optical thicknesses is compared against the aerosol optical thickness retrieved from the O_2 A band. Thus, PMAp aerosol optical thickness is spatiotemporally collocated with the spectrometer measurements that we use for our O_2 A band retrievals. Note that at the time of writing, PMAp aerosol optical thickness was only available for sea pixels. We have also compared retrieved aerosol optical thickness with MODIS Terra aerosol optical thickness, which is available for land surfaces as well, but the correlation was worse. This is probably due to the different overpass times of the Metop-A and Terra satellites.

It is important to remark that an absolute validation of retrieved aerosol optical thickness is neither attempted here nor expected, because PMAp aerosol optical thickness is reported at a different wavelength and our optical thickness is an effective quantity, which holds for the aerosol model assumed in the retrieval (see Sect. 2). However, if our O_2 A band retrieval is indeed picking up an aerosol signal, we do expect a significantly positive correlation with PMAp aerosol optical thickness when many different aerosol scenes are included in the comparison. PMAp aerosol optical thickness correlates significantly with retrieved O_2 A band aerosol optical thickness when not fitting the surface albedo (left panel of Fig. 8). When fitting the surface albedo, the situation becomes less clear. The data appear to separate into two clusters (which is the reason why a linear regression is not performed) and retrieved O_2 A band aerosol optical thickness for the denser one is significantly lower than PMAp aerosol optical thickness. We come back this observation in Sect. 11.

8 Algorithm sensitivities for GOME-2A target pixels

In this section, we illustrate a number of algorithm sensitivities using real data retrievals. Because the radiative transfer calculations are time-consuming, we select a target GOME-2A pixel for every scene and perform sensitivity experiments for this set of pixels only. We discuss the effect on con-

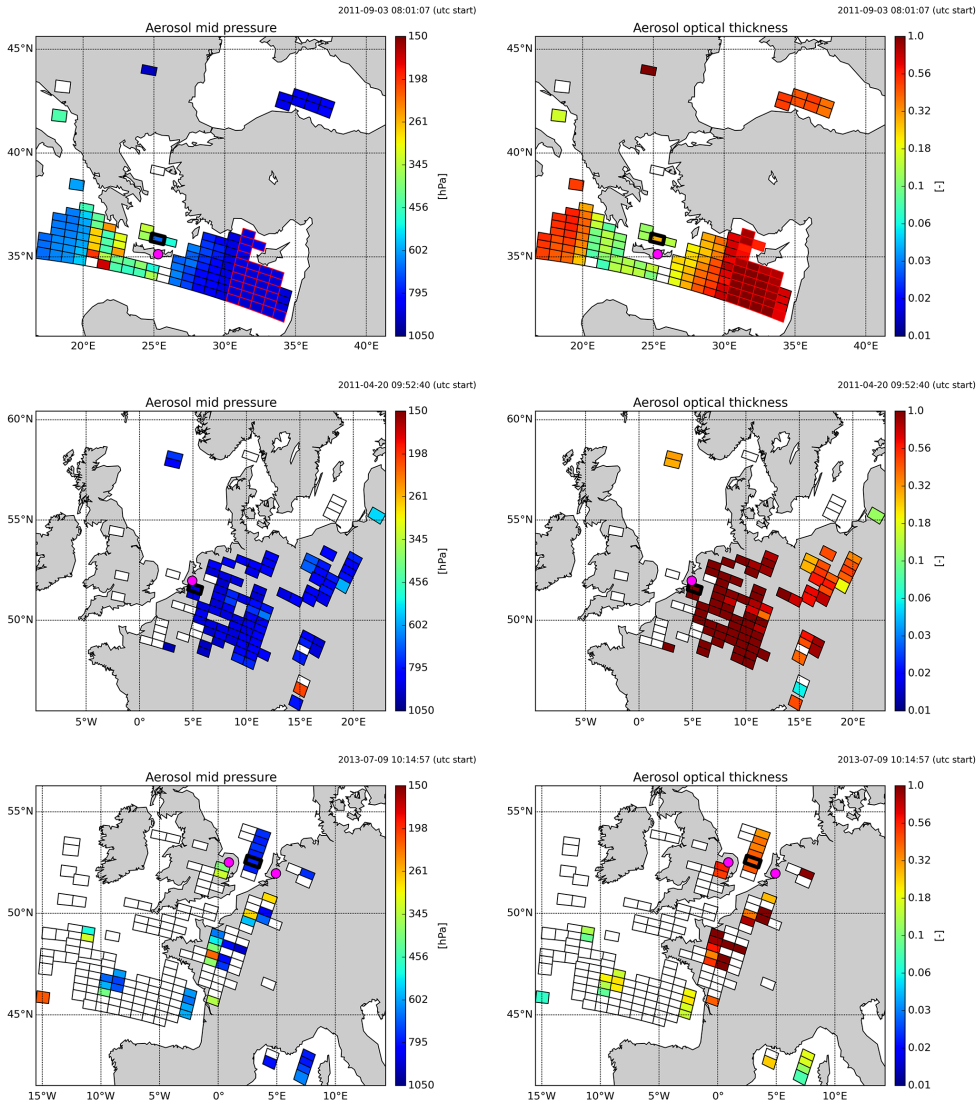

Figure 6. Retrieved aerosol layer mid pressure (left column) and aerosol optical thickness (right column) for three representative GOME-2A scenes (rows) when the surface albedo is fixed in retrieval. The depicted aerosol scenes are (from top to bottom) scene 01, scene 03, and scene 04 from Table 4. Next to P_{mid} and τ (760 nm), a temperature offset ΔT is fitted. The layer's assumed pressure thickness is 50 hPa. The model value for the surface albedo is taken from the MERIS black-sky albedo climatology (Popp et al., 2011). Pixels that had no converging retrieval for any of the six attempted runs (i.e., for any of the different sets of initial values) are plotted in white. Missing pixels are pixels that did not pass cloud filtering. The target pixel that is used in the sensitivity experiments of Sect. 8 is depicted with a thick black border. Quadrangles with red borders indicate pixels that are inside the sun glint region. Finally, spatial locations of the lidar measurements are shown with purple dots. Values outside the ranges depicted are clipped.

vergence and the retrieval solution of the assumed aerosol model, scaling of the oxygen absorption cross section and fitting of a temperature offset, fitting of the surface albedo, and fitting of a stray light offset or a fluorescence emission.

In the first experiment we investigate the effect of the assumed aerosol model. The retrieval setup is the same as in Sect. 7 and the surface albedo is fixed in retrieval (as in Fig. 6) or it is retrieved (as in Fig. 7). Figure 8 shows the fraction of converged runs, retrieved aerosol layer mid pressure, aerosol optical thickness and surface albedo (only wavelength node 758 nm is shown) for three different aerosol models assumed in retrieval when the surface albedo is fitted. Figure 10 shows retrieved aerosol layer mid pressure and aerosol optical thickness for the same three aerosol models when the surface albedo is not fitted. These aerosol models are (i) a particle with a single scattering albedo of 0.95 and a Henyey–Greenstein phase function with asymmetry parameter of 0.7 (the default model), (ii) a particle with a single scattering albedo of 1.0 and a Henyey–Greenstein phase function with asymmetry parameter of 0.8, and (iii) a Mie

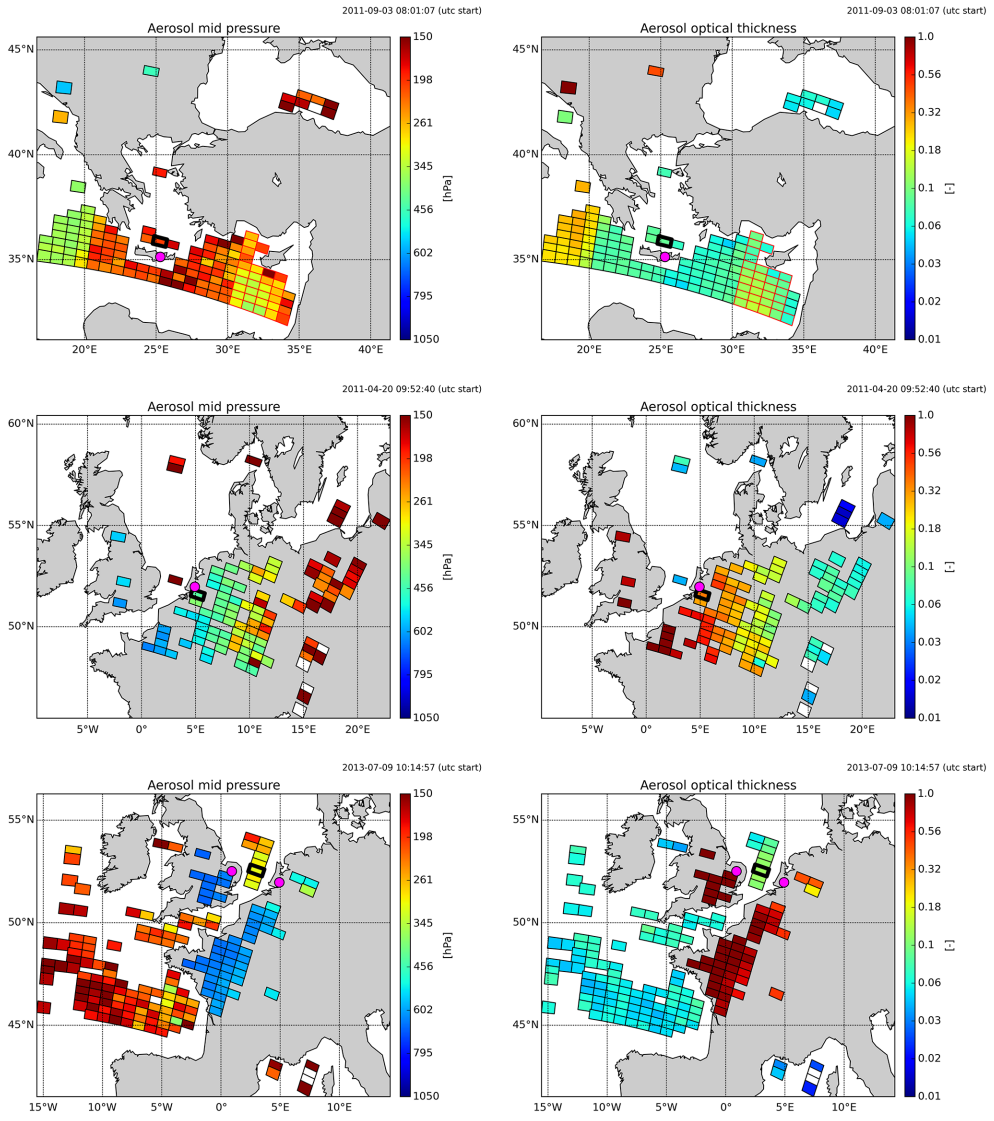

Figure 7. Retrieved aerosol layer mid pressure (left column) and aerosol optical thickness (right column) for the same GOME-2A scenes (rows) as in Fig. 6 when including the surface albedo in the state vector. Next to P_{mid} and τ (760 nm), the surface albedo A_{S} and a temperature offset ΔT are fitted. Other settings are the same as in Fig. 6.

particle with single scattering albedo at 760 nm of 0.97 and a phase function with asymmetry parameter of 0.58. The latter model is the fine mode weakly absorbing aerosol type from the aerosol-CCI project (see De Leeuw et al., 2015). These aerosol models are chosen for no other reason than that they show some variability in microphysical properties. In this experiment and in all other sensitivity experiments described in Sect. 8, retrieval is attempted for four initial values of the aerosol layer mid pressure and three initial values of the optical thickness (12 runs in total). The fraction of converged runs is thus defined as the number of converged runs divided by 12. Finally, retrieved parameter values for the solution with the smallest χ^2-value are shown and whiskers indicate the maximum to minimum range of retrieval solutions.

In the first place, this experiment confirms the observation made before in the simulation study of Sect. 2 that the assumed aerosol model has only a moderate effect on retrieved aerosol pressure. Interestingly, when the same experiment is repeated but without fitting the surface albedo, we see that the effect of the assumed aerosol model remains quite moderate for many pixels (although a number of other pixels now fail to have converging runs). In the second place, we see that retrieval is very stable. Most of the 12 runs (i.e., retrieval attempts for different sets of initial values) converge and they usually converge to the same retrieval solution.

Next, Fig. 11 shows residuals for all converged runs for all target pixels plotted on top of each other. The default aerosol model is assumed and these retrievals thus correspond to the

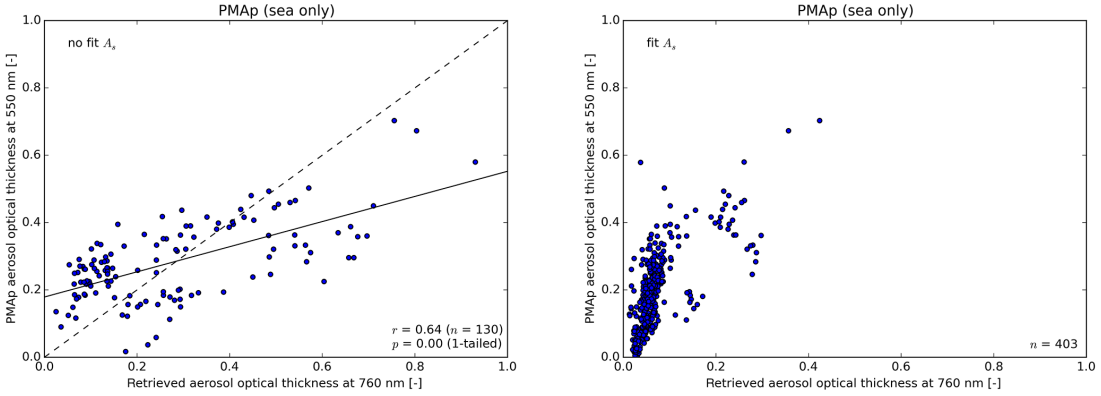

Figure 8. PMAp aerosol optical thickness at 550 nm against aerosol optical thickness retrieved from the O_2 A band measured with GOME-2A when the surface albedo is not fitted (left panel) and when it is (right panel). In these plots, PMAp aerosol optical thickness is the mean of valid PMAp retrievals (at least one) for PMD subpixels within the GOME-2A spectrometer's footprint.

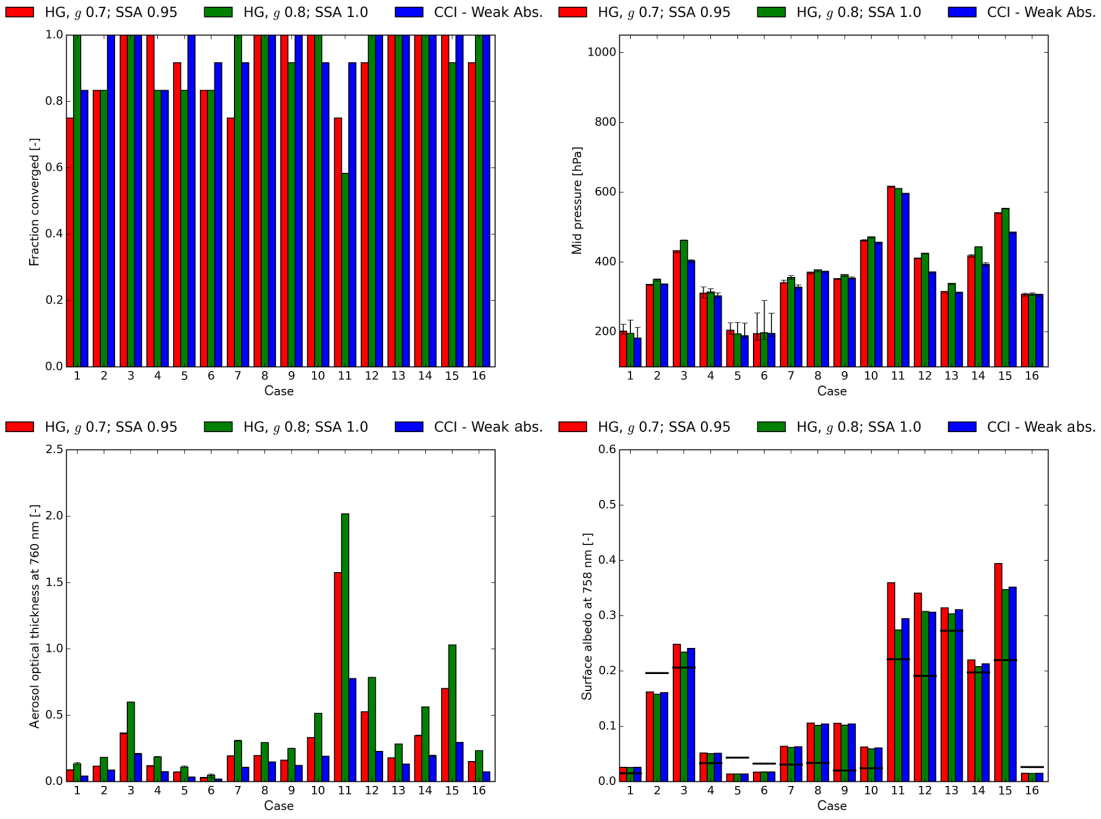

Figure 9. Fraction of converged runs (top left), retrieved aerosol layer mid pressure (top right), retrieved aerosol optical thickness (bottom left) and retrieved surface albedo at 758 nm (bottom right) for 16 GOME-2A target pixels and three different aerosol models. For a description of these aerosol models, see the main text. The first aerosol model is the model also assumed in the scene retrievals. All other details of the retrieval setup are the same as in Sect. 7 and the surface albedo is fitted (as in Fig. 7). Thus, retrieval results for cases 01, 03 and 04 shown here with red bars are the same as retrieval results for highlighted target pixels in the scenes of Fig. 7. Also, retrieval is now attempted for 12 different sets of initial values (as opposed to six in the scene retrievals). Whiskers for retrieved parameter values indicate the maximum to minimum range of retrieval solutions. Often, the range of retrieval solutions for different initial values is so small that whiskers are not visible. Finally, black horizontal line segments in the bar plot for the surface albedo show the climatological (a priori) value from the MERIS black-sky albedo climatology.

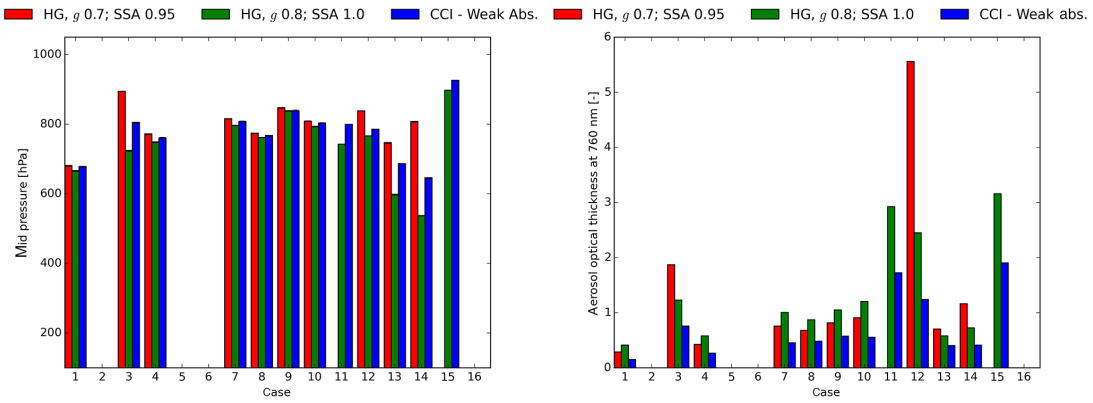

Figure 10. Retrieved aerosol layer mid pressure (left) and aerosol optical thickness (right) for 16 GOME-2A target pixels and three different aerosol models. Details are the same as in Fig. 9, except that now the surface albedo is fixed in retrieval (as in Fig. 6).

baseline retrieval setup of Sect. 7. The left panel shows relative residuals when the surface albedo is fixed in retrieval and the right panel when the surface albedo is fitted. Relative residuals are defined as $(R_{\text{meas}} - R_{\text{fit}})/R_{\text{meas}} \cdot 100\,\%$. It is clear that residuals have a distinct spectral structure, which can be a starting point for future investigations. We have residuals up to about 24 % when the surface albedo is not fitted and residuals up to about 8 % when the surface albedo is retrieved. It should be noted, however, that relative residuals peak inside the absorption band where reflectances can be up to a factor of 10 smaller than in the continuum. In particular, the difference between the two conditions is mainly a peak in the R-branch around 760.5 nm, but otherwise, relative residuals are very similar in magnitude. Absolute fit residuals are indeed spectrally more flat. Figure 12 shows the measured and modeled reflectance spectra and the absolute residuals for two example pixels. From these plots the difference between fitting and not fitting the surface albedo is less pronounced. Interestingly, absolute residuals when not fitting the surface albedo appear to have a slope, which is perhaps related to an incorrect wavelength dependence of the surface albedo as this dependence is basically determined by the surface albedo climatology.

In the second experiment we investigate the effect of scaling the oxygen absorption cross section and fitting of a temperature offset. Recall that in the default retrieval setup, the calculated oxygen absorption cross section is increased by 3 % in agreement with Butz et al. (2013) and Crisp et al. (2012), and an offset to the a priori ECMWF temperature profile is fitted. Figure 13 shows the fraction of converged runs and retrieved aerosol layer mid pressure for three experimental conditions. In the first condition, neither the oxygen absorption cross section is scaled nor a temperature offset is fitted. In the second condition, the oxygen absorption cross section is increased by 3 %. In the third condition, also a temperature offset is fitted. This latter condition then corresponds to the default retrieval setup.

We observe that convergence for the set of target pixels improves when the oxygen absorption cross section is scaled and when a temperature offset is fitted. In fact, for two target pixels none of the 12 runs converges in the base condition, while all 12 runs converge when the absorption cross section is scaled and a temperature offset is fitted. The significant improvement of convergence is the reason why we did both in the default retrieval setup for the scene retrievals. There are small but systematic effects on retrieved parameter values; this is generally expected, considering the high correlations between errors in fit parameters discussed above. Furthermore, we find that retrieved temperature offsets are always negative and ranging from about -4 to -8 K (not shown). This means that for every GOME-2A pixel the entire a priori temperature profile, which we constructed from ECMWF reanalysis data at high spatial resolution, is shifted to lower temperatures by this amount in the retrieval. Apparently, fitting a temperature offset compensates for model errors other than remaining inaccuracies in meteorological data, as the temperature offset would have been random and much smaller in magnitude in that case. (Note that we are retrieving aerosol in cloud-free, hence meteorologically stable, conditions.) Finally, we remark that, although convergence improves, retrievals that converged in all three conditions do not show an overall and systematic decrease in spectral fit residuals. Some peaks slightly decrease but other peaks slightly increase.

We have also experimented with fitting stray light (i.e., additive top-of-atmosphere radiance offset) and a fluorescence emission (i.e., additive contribution to the upwelling radiance field at the surface). The actual spectral shape of a presumed stray light offset at the O_2 A band, or rather stray light that remains after corrections have been applied in the level-1b processor, is unknown and can be quite variable because of the large dynamic range of the radiance spectrum. In these first investigations, we have therefore simply assumed that the stray light offset is spectrally constant. A fluorescence

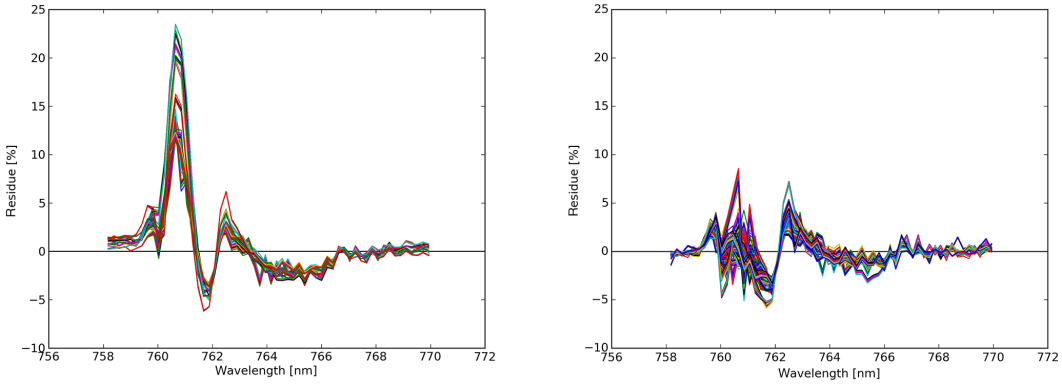

Figure 11. Fit residuals for all converged runs for the 16 GOME-2A target pixels. The default retrieval setup of Sect. 7 is used. Left panel: surface albedo not fitted (see Fig. 6); right panel: surface albedo fitted (see Fig. 7). Relative residues are defined as $(R_{\mathrm{meas}} - R_{\mathrm{fit}})/R_{\mathrm{meas}} \cdot 100\,\%$.

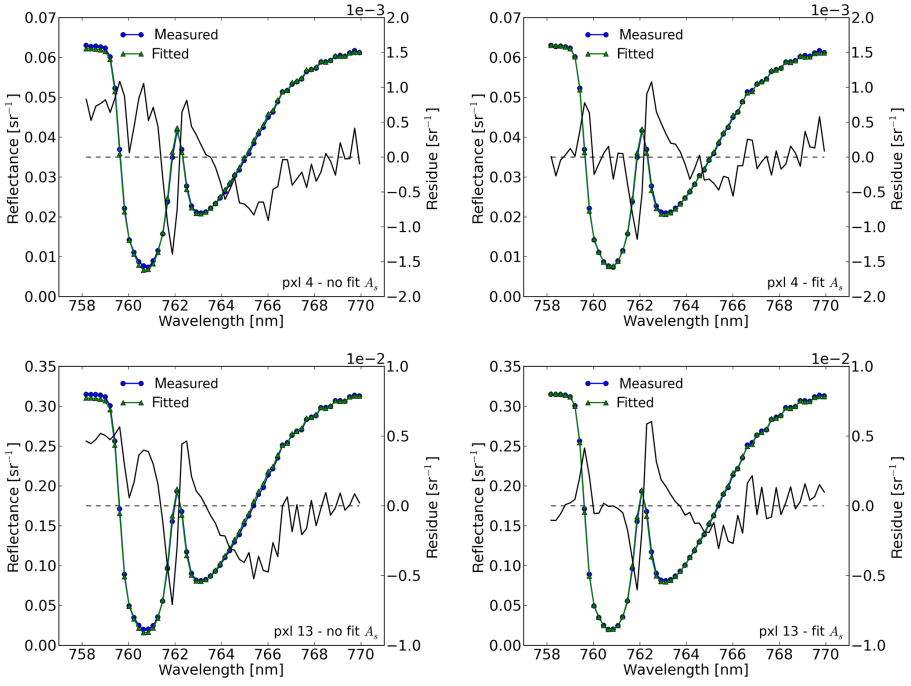

Figure 12. Measured and modeled reflectance spectra for two example GOME-2A target pixels. Top row: pixel over sea (target pixel 04); bottom row: pixel over land (target pixel 13). Left column: surface albedo not fitted; right column: surface albedo fitted. Absolute residues are defined as $R_{\mathrm{meas}} - R_{\mathrm{fit}}$. The default retrieval setup of Sect. 7 is used and the run with the smallest χ^2-value is shown.

emission is typically spectrally smooth and here allowed to depend linearly on wavelength across our fit window.

When fitting the surface albedo, including a stray light offset in the state vector does not show a systematic improvement of the retrieval. The fraction of converged runs stays the same or perhaps slightly decreases. At the same time we do not observe a systematic decrease of fit residuals. Interestingly, we find that the retrieved radiance offset is typically quite large and negative (ranging from 0 to −5 % and on average −2.5 % of the continuum radiance). A negative offset means that light is removed from the spectrum. At the same time, we see that retrieved mid pressure is systematically lower by on average 85 hPa (range: 0 to 150 hPa). The relative contribution of spectrally constant stray light to the reflectance spectrum is largest inside the absorption band. Any errors in retrieved spectral stray light (for example, because the spectral model is inaccurate) may thus easily interfere with retrieved aerosol layer mid pressure. Since there is no systematic improvement of convergence or residuals, and because the spectral shape of possible stray light is presently unknown to us, we have decided to not fit stray light in the default algorithm setup for the scene retrievals of Sect. 7.

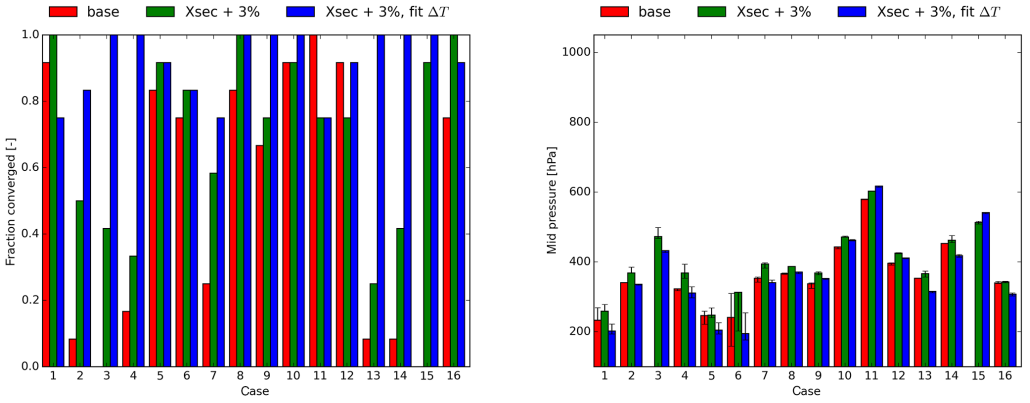

Figure 13. Fraction of converged runs (left) and retrieved aerosol layer mid pressure (right) for 16 GOME-2A target pixels and three experimental conditions. In the third experimental condition, the oxygen absorption cross section is increased by 3 % and a temperature offset is fitted. This condition corresponds to the default retrieval setup used for the scene retrievals of Sect. 7. In the second experimental condition, only the oxygen absorption cross section is scaled, but the temperature profile is fixed in retrieval. In the first experimental condition, neither the oxygen absorption cross section is scaled nor a temperature offset is fitted. All other details of the retrieval setup are the same as in Sect. 7 and the surface albedo is fitted (as in Fig. 7).

A similar observation is made when including fluorescence emissions in the state vector instead of a stray light offset. There is no systematic effect on convergence. For some pixels the fraction of converged runs increases, for some it stays the same, and for some it decreases. Also, no effect on spectral fit residuals is found. Interestingly, retrieved fluorescence emissions are always negative. The emission at 758 nm ranges from 0 to -2×10^{12} and is -1×10^{12} photons $s^{-1}\,cm^{-2}\,sr^{-1}\,nm^{-1}$ on average. The magnitude of the retrieved emission at 770 nm is on average 2.5 times as large. In contrast, for chlorophyll fluorescence one would expect positive values that are smaller in magnitude at the longer wavelength node (e.g., Amoros-Lopez et al., 2008). Also, significant (negative) fluorescence emissions are retrieved for sea pixels, although they are smaller in magnitude than for land pixels. Because of these observations, we hypothesize that retrieved fluorescence emissions have the same origin as retrieved stray light offsets. A difference between stray light offsets and fluorescence emissions is that the latter bears an O_2 A band signature. The effect of fitting fluorescence emissions on retrieved aerosol pressure is indeed different. Now, retrieved aerosol layer mid pressures are systematically higher by an amount ranging from 20 to 175 hPa and being 110 hPa on average.

Fitting stray light does have an impact on residuals when the surface albedo is fixed in retrieval, which is perhaps expected. As explained above, relative residuals show a large peak near 760.5 nm in that case. When we fit a stray light offset in this experimental condition, the peak disappears. However, convergence does not improve and there is a strong interaction with retrieved aerosol layer mid pressure. For those reasons, we also do not fit a stray light offset when we keep the surface albedo fixed in retrieval, and we accept the large fit residual inside the O_2 A band illustrated in the left panel of Fig. 11.

The accuracy of a priori information about the surface albedo becomes more important when the surface albedo is not fitted. So far, we have used the MERIS black-sky albedo climatology (Popp et al., 2011). For sea pixels this climatology is filled with values from the GOME Lambertian-equivalent reflectivity climatology (Koelemeijer et al., 2003). GOME's ground pixels are usually 40 km by 320 km and hence there is a high chance of cloud contamination of the climatology. As a first investigation into the effect of the surface albedo climatology used to provide a priori values, we have tested the effect on retrieval when using the ADAM database (ADAM: a surface reflectance DAtabase for ESA's earth observation Missions; ESA, 2013) instead of the MERIS climatology. The ADAM database provides climatological values (monthly, 0.1° by 0.1°) for the Bidirectional Reflectance Distribution Function (BRDF). We retrieved the BRDF from the database for the specific observation geometry of the GOME-2A target pixel and used it as a Lambertian-equivalent reflectivity in our O_2 A band retrieval. Unfortunately, we do not observe an improvement of the comparison of retrieved aerosol layer mid heights with lidar measurements of the aerosol extinction profile (to be discussed below), but we have to remark that only six out of the 16 target pixels had converging runs for both climatologies so the statistical basis for this finding is limited.

To conclude this section, we have discussed various experiments exploring a number of algorithm sensitivities. However, more research is needed to substantiate the observations and make conclusive and quantitative statements. Particularly, more pixels should be included in future retrieval experiments to improve the statistics and see whether our findings are robust.

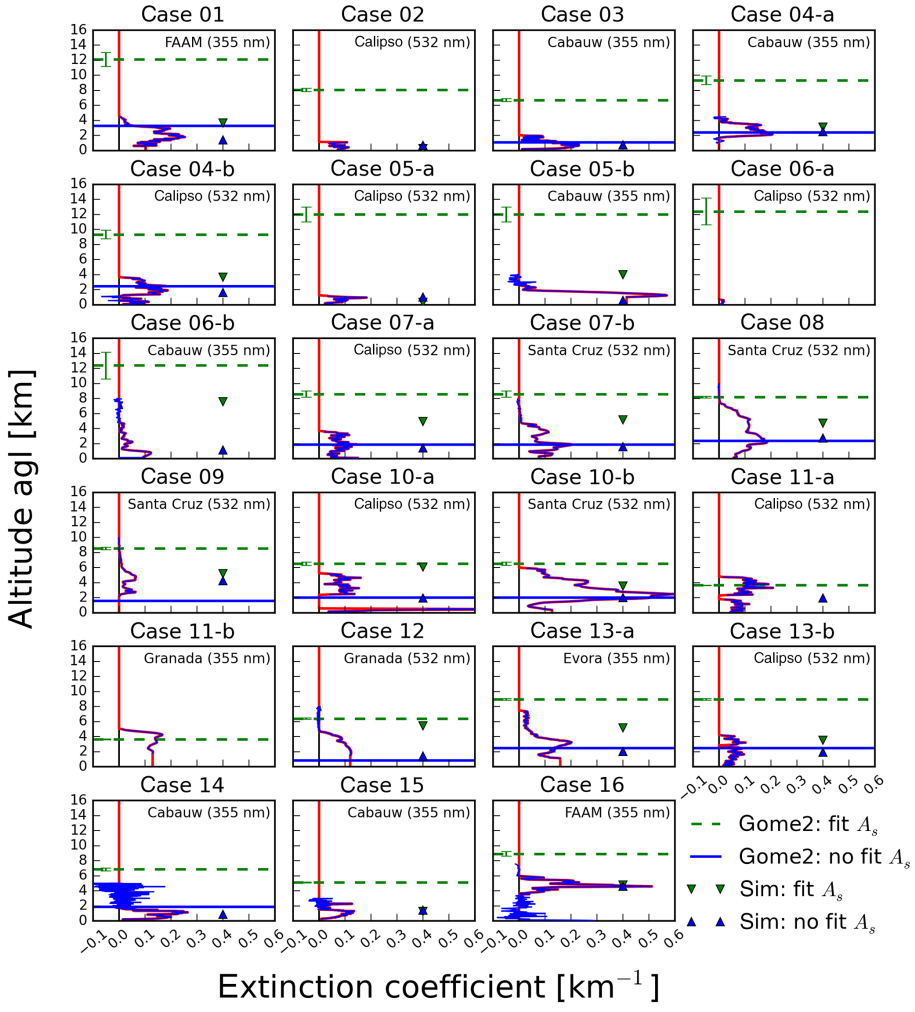

Figure 14. Comparison of retrieved aerosol layer mid heights for the 16 GOME-2A target pixels with aerosol extinction profiles measured by the lidars listed in Table 5. For some target pixels, two lidar measurements are included in the comparison. An overview of the spatial layout of target pixels and locations of the lidar observations is depicted in Fig. 5. Aerosol extinction profiles are given at 355 or 532 nm for altitudes above ground level (a.g.l.). Profiles indicated with thin blue lines are the data provided by the lidar teams; profiles indicated with thick red lines are inter- and extrapolated and smoothed profiles used in the retrieval simulations. Horizontal lines are GOME-2A retrieved aerosol layer mid altitudes (green dashed: surface albedo is fitted; blue solid: surface albedo is fixed in retrieval). The retrieval setup is the same as in the scene retrievals of Sect. 7. Missing lines indicate that the GOME-2A retrieval did not converge. Finally, triangles indicate retrieved aerosol layer mid altitudes when the aerosol extinction profiles shown in red are used to simulate a measurement (green downward triangles: surface albedo is fitted; blue upward triangles: surface albedo is fixed in retrieval). Missing data points indicate that the simulated retrieval did not converge. For details of this simulation, see the main text.

9 Comparison with lidar observations

Figure 14 shows a comparison of retrieved aerosol layer heights with lidar observations for every GOME-2A target pixel and for the default retrieval setup of Sect. 7. The spatial layout of target pixels and lidar measurements is shown in Fig. 5, and a description of each lidar measurement and its spatiotemporal distance to the corresponding target pixel is given in Table 5. Spatial or temporal distances to the target pixel can sometimes be quite large, in which case we have tried to include a second lidar measurement in the comparison. Aerosol extinction profiles are given at 355 or at 532 nm. No conversion to wavelengths of the O_2 A band is made, because at this stage we are mainly interested in the shape (or layering) of the extinction profile, which we assume to be the same at 760 nm. Extinction profiles indicated with thin blue lines are the data provided by the lidar teams; profiles indicated with thick red lines are inter- and extrapolated and smoothed profiles to be further used in retrieval simulations discussed below. Also depicted (with horizontal lines) are retrieved aerosol layer mid altitudes for the GOME-2A target pixels. We converted aerosol layer mid pressures

into altitudes using the corresponding ECMWF (a priori) temperature profiles rather than the retrieved (a posteriori) temperature profiles because the former are probably more accurate (see discussion of retrieved temperature offsets in Sect. 8). Finally, error bars indicate the a posteriori 1σ error in retrieved altitude. Errors are only occasionally large enough to be visible in theses plots. We remark that precision errors are calculated from the nominal level-1b noise errors (see Sect. 6.2). It can be anticipated based on the discussion of correlations in Sect. 2 that the total error budget is dominated by accuracy errors.

Typical collocation criteria used by EARLINET stations for correlative measurements with CALIPSO are on the order of 100 km and 2 h (e.g., Mona et al., 2009; Pappalardo et al., 2010). Spatiotemporal collocation of GOME-2A target pixels with lidar measurements (Table 5) is then already quite reasonable for most (but not all) extinction profiles considering the size of GOME-2A pixels. However, as mentioned before, we are not attempting a full validation of our retrieval results but only do a first comparison to better understand the effects that we have found, in particular the effect of treatment of the surface albedo. In Sect. 7, we saw that retrieved aerosol pressures are often very low and can attain unrealistic values when the surface albedo is fitted. On the other hand, retrieved aerosol pressures are much more realistic when the surface albedo is not fitted (although convergence is worse in that case). Retrieved aerosol heights can now be compared against a number of example lidar profiles that are to some extent representative of general aerosol conditions in the respective aerosol scene. The main observation in Fig. 14 is that retrieved mid altitudes when fitting the surface albedo are indeed too high for most cases. However, retrieved mid altitudes when not fitting the surface albedo typically show values that are probably representative of actual aerosol extinction profiles. Thus, the observations made in Sect. 7 are supported by the comparison with lidar measurements.

In detail, focusing on retrieved mid altitudes when not fitting the surface albedo (blue horizontal lines), we see that altitudes are usually inside the corresponding extinction profile (cases 03, 04-a and 04-b, 07-a and 07-b, 08, 10-a and 10-b, 13-a and 13-b). For two cases they are somewhat near the top of the profile (cases 01 and 14), for another case the retrieved altitude is in the lower part of the corresponding profile (case 12) and for again another case it is below the profile (case 09). In the latter case orographic effects due to transport over the mountainous island of Tenerife may have played a role, but we could not confirm this with preliminary trajectory analyses. Overall, the results suggest that retrieved mid altitude typically is some sort of weighted average of the actual extinction profile in this experimental condition, as has also been argued and reported for cloud retrieval schemes that resemble our algorithm setup (see Sect. 11). We do not further investigate in detail the relation between retrieved GOME-2A layer mid heights and the lidar profiles here. This should be the topic of a dedicated and more comprehensive validation study that includes many more cases for better statistics.

We have also used the aerosol extinction profiles of Fig. 14 in retrieval simulations to investigate the isolated effect of profile shape on retrieved aerosol layer mid height. The lidar aerosol extinction profiles are discretised and used to simulate a spectrum for TROPOMI instrument specifications (see Sect. 2). A possible wavelength dependence of the aerosol extinction coefficient is ignored (i.e., an Ångström coefficient of zero is assumed), the temperature profile of the corresponding GOME-2A target pixel is used to convert altitudes into pressures and also the observation geometry is taken from the target pixel. Finally, the same aerosol model assumed in the GOME-2A retrievals is used also for these simulations. Missing data points indicate that retrieval did not converge, which happened in a few cases. The results of these simulations further support the observations made above. Retrieved mid altitude is often higher when fitting the surface albedo compared to when not fitting the surface albedo. In the latter case, retrieved mid altitude seems much more representative of the true profile. We will further investigate this finding in the following section. As a final remark, from Fig. 14 it appears that when fitting the surface albedo, aerosol layer mid altitudes from retrieval simulations are systematically lower than altitudes from the GOME-2A retrievals. It is not clear whether this effect is significant and related to instrument effects or perhaps to the wavelength dependence of the aerosol extinction coefficient being ignored here (leading to a possible overestimation of aerosol extinction at the O_2 A band).

10 Retrieved layer pressure when two scattering layers are present

In the previous sections, we found on the one hand that treating the surface albedo as a model parameter, whose value is taken from a climatology, leads to many non-converging retrievals. Interestingly, we also observed that retrievals that did converge showed retrieved aerosol layer mid pressures that appear representative of the actual aerosol extinction profiles. Of course, next to noise errors also systematic errors, such as an error in the assumed aerosol model, contribute to the total error budget. On the other hand, including the surface albedo in the state vector led to a fraction of converged retrievals close to one, but retrieved aerosol layer mid pressures in that case were very low and often the layer appeared to be retrieved above the aerosols. In this section, we show results from retrieval simulations investigating the effect of a second interfering scattering layer on retrieved pressure of a target aerosol layer to further understand these findings.

The forward model is the same as used for the GOME-2A retrievals, except that now the TROPOMI instrument model is used. Also, the target layer (in simulation and retrieval)

and the interfering layers contain purely scattering particles for ease of interpretation, but other settings are the same as in the simulation study of Sect. 2. The elevated target layer is between 700 and 600 hPa and has an optical thickness at 760 nm of 0.3. Aerosols have a single scattering albedo of 1.0 and a Henyey–Greenstein phase function with asymmetry parameter of 0.7. The surface has a constant albedo of 0.03 (sea) or 0.20 (land). Fit parameters are the pressure of an assumed single aerosol layer with fixed pressure thickness (here 100 hPa), the aerosol layer's optical thickness and sometimes also the surface albedo. We illustrate the effect of two scattering layers on retrieved layer pressure with two representative examples. The left column of Fig. 15 shows retrieved layer mid pressure when an interfering cirrus layer is present. The cirrus layer is between 500 and 440 hPa (about 6 to 7 km) and has a cloud fraction of one, and cirrus particles have a single scattering albedo of 1.0 and a Henyey–Greenstein phase function with asymmetry parameter of 0.8. The right column of Fig. 15 shows retrieved layer mid pressure when an interfering boundary layer is present. Boundary layer aerosols, which have the same properties as the aerosols in the target layer, are between the surface and 100 hPa above the surface.

When above the elevated target layer an interfering scattering layer is present, such as a cirrus layer, for example (left column of Fig. 15), retrieved aerosol layer mid pressure is between the target layer and the interfering layer. The higher the optical thickness of the interfering layer, the more retrieved aerosol layer pressure tends towards this second layer. Although both layers are elevated, whether the surface albedo is fitted (solid lines) or not (dashed lines) affects retrieved layer pressure. This is perhaps surprising but it is understandable in view of the high correlations between errors in fit parameters (Sect. 2): a model error in the assumed aerosol profile (one vs. two scattering layers) affects retrieved surface albedo and this in turn has an effect on retrieved aerosol layer pressure. Here, the surface albedo is retrieved at a value slightly higher than its true value. One may argue that retrieved aerosol layer pressure when the surface albedo is not fitted but held at its model value is the true average pressure. Then, in the left column of Fig. 15 fitting the surface albedo causes biases in retrieved aerosol layer pressure up to 50 hPa (cirrus optical thickness of 0.2, sea) and 90 hPa (cirrus optical thickness of 0.2, land), which is the difference between dashed and solid lines.

When boundary layer aerosols are added to the scene (right column of Fig. 15), retrieved layer pressure is between the two layers if the surface albedo is not retrieved. However, if the surface albedo is fitted, retrieved layer pressure moves away from the boundary layer. Fitting the surface albedo now causes large biases in retrieved aerosol layer pressure. For example, for a boundary layer optical thickness of 0.05 to 0.1, which are common values, retrieved pressure of the target layer (optical thickness of 0.3) is biased by about 115 to 155 hPa (difference between dashed and solid lines). Biases are larger and non-convergences occur more often for the brighter surface. Also, the retrieved surface albedo is above its true value, while the retrieved optical thickness is biased low. Finally, we remark that residues in both conditions increase when more and more boundary layer aerosols are added to the scene (not shown).

We hypothesize that the following mechanism is at work. Although the two columns of Fig. 15 seemingly show such diverging results, the effects of a second interfering scattering layer, be it cirrus or boundary layer aerosols, are actually similar in a qualitative sense. Yet quantitatively, the effect is much more pronounced for boundary layer aerosols. Suppose we start the simulations with only one scattering layer (i.e., the elevated target layer). The forward model used in retrieval captures this situation well of course and all parameters are retrieved at their true values. Now we begin adding cirrus or boundary layer aerosols. Remember that we consider purely scattering aerosols throughout. To get agreement in the continuum, the aerosol optical thickness of the single layer assumed in the retrieval is increased when the surface albedo is held fixed at its true value. If the surface albedo is fitted, also this parameter will increase to a certain extent because errors are correlated. But the penalty for increasing the surface albedo is that the absorption band becomes too deep. To also fit reflectances inside the absorption band then, the aerosol layer has to be moved to lower pressures to compensate for this in the retrieval. Hence, retrieved pressures in Fig. 15 are lower when the surface albedo is fitted. The particular combination of aerosol optical thickness, surface albedo, and aerosol layer pressure that eventually results depends on the fit. However, it is easier to attribute aerosol scattering to surface reflection when aerosols are closer to the surface (indeed, the surface albedo reacts more strongly in that case). The pressure difference between boundary layer aerosols and the surface has yet to be compensated for, and this causes the aerosol layer to be retrieved above the elevated target layer.

11 Discussion and conclusions

In this paper, we have presented and discussed an algorithm setup for retrieval of aerosol layer height from spectral measurements of the oxygen A band. The algorithm has been applied to GOME-2A spectra in a number of systematic and extensive case studies, retrieved aerosol layer height has been compared against lidar measurements, and subsequent retrieval simulations have been performed to further understand the GOME-2A retrieval results. Retrieval of aerosol height information from the O_2 A band is challenging, as becomes clear also in this paper, and algorithm development will continue in the coming time. In this work, we have identified many starting points for further investigations. We believe that we have made a step ahead from the sensitivity studies and the limited number of case studies on O_2 A band

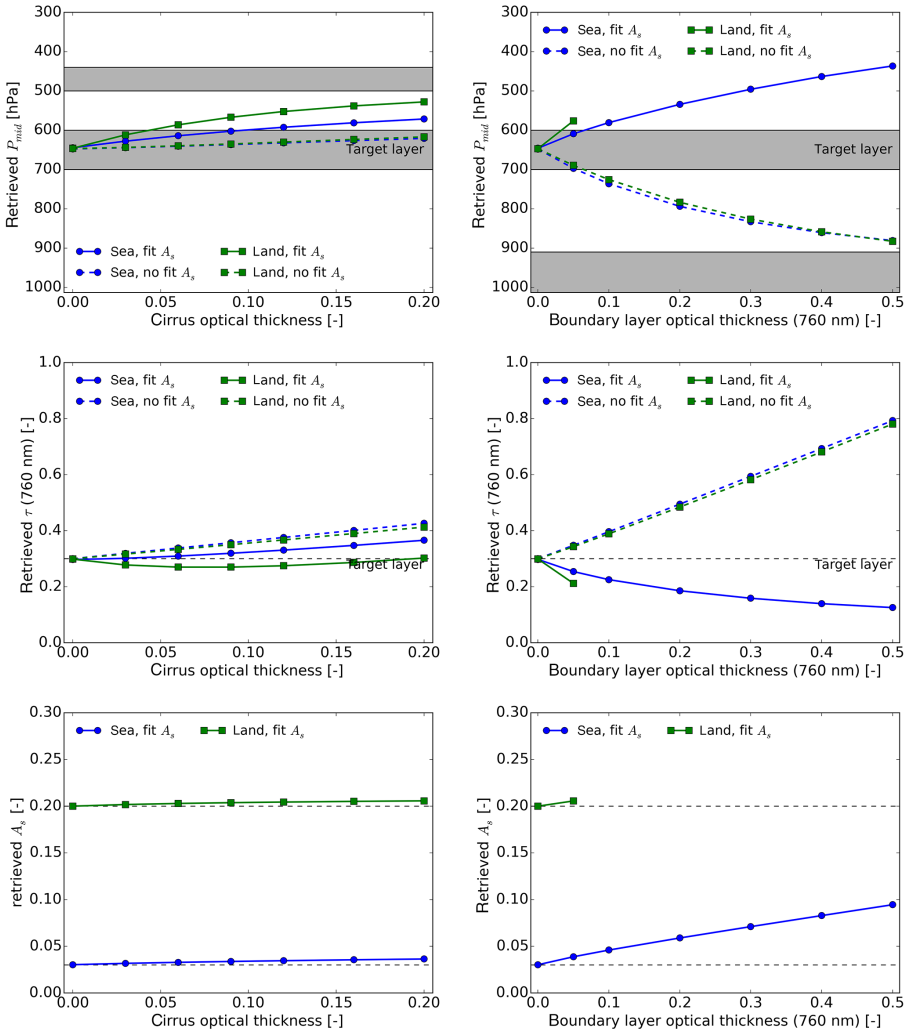

Figure 15. Results of retrieval simulations showing retrieved mid pressure (top row) of an assumed single aerosol layer with fixed pressure thickness, the layer's retrieved optical thickness (middle row) and the retrieved surface albedo (bottom row) when in the forward simulation two scattering layers are present. Retrieved parameter values are shown as a function of the optical thickness of the interfering layer. The four plot lines correspond to sea (blue, circles) and land (green, squares) and to not fitting (dashed lines) and fitting (solid lines) the surface albedo. The target layer has an optical thickness of 0.3. Aerosols have a single scattering albedo of 1.0 and a Henyey–Greenstein phase function with asymmetry parameter of 0.7. The interfering layer is a cirrus layer (left column) or a boundary layer containing aerosols (right column). The cirrus layer has a cloud fraction of 1.0, and cirrus particles have a single scattering albedo of 1.0 and a Henyey–Greenstein phase function with asymmetry parameter of 0.8. Missing data points indicate non-converging retrievals. The solar zenith angle is 50° and the viewing direction is nadir. All other settings are the same as in the simulation study of Sect. 2 (see also Figs. 1 and 2).

aerosol retrieval that have appeared so far. The definitive answer to the question of what an O_2 A band aerosol height retrieval is eventually capable of, however, is yet to be given. The following main observations and conclusions emerge from the GOME-2A retrievals and the retrieval simulations.

Whether or not the surface albedo is retrieved simultaneously with aerosol layer height and optical thickness can have a significant impact on the retrieval outcome. When the surface albedo is fitted, convergence of the GOME-2A scene retrievals is good but we find that retrieved aerosol layer pressures are very low. With this in mind, we have applied a very strict filtering on cirrus using, among other tests, a dedicated test in the thermal infrared. Therefore, we can rule out cirrus contamination of the relatively large GOME-2A pixel as an explanation for the systematically low aerosol pressures, and we hypothesize that these are more likely linked to a characteristic of the retrieval algorithm itself. Indeed, retrieved aerosol layer heights attain realistic values when the surface albedo is removed from the state vector. The observation of realistic aerosol layer heights (in case the surface albedo is fixed in retrieval) is further supported by the comparison of retrieved aerosol layer heights with lidar profiles for a se-

lected set of GOME-2A target pixels. The drawback of not fitting the surface albedo, however, is a decrease in convergence, which is probably caused by, among other things, inaccuracies in climatological values.

In subsequent retrieval simulations we investigated the effect of the shape of the aerosol extinction profile in isolation. As a first step, we used realistic extinction profiles to simulate measured spectra while assuming the single-layer model in the retrieval. Again, we find that retrieved aerosol layer pressures are typically biased low when fitting the surface albedo compared to when not fitting this parameter. As a second step, we narrowed down the retrieval simulations to investigating the effect of two scattering layers. Particles are now taken purely scattering in both simulation and retrieval so that results can be interpreted more easily. From these retrieval simulations, we learn that a model error in the extinction profile is partly absorbed by the surface albedo. This is expected as errors in fit parameters are correlated. We see that the retrieved particle optical thickness underestimates the true total particle optical thickness and that the retrieved surface albedo overestimates the true surface albedo. At the same time, the aerosol layer is retrieved at lower pressures in agreement with the GOME-2A retrievals. In the case of boundary layer aerosols, however, the corresponding effect on retrieved aerosol layer height is substantial to the extent that the aerosol layer is eventually retrieved above the two-layer system. This is perhaps unexpected given previous cloud validation studies investigating multiple-layer clouds (e.g., Wang and Stammes, 2014; Joiner et al., 2010, 2012; Lelli et al., 2012; Sneep et al., 2008; Vasilkov et al., 2008). These studies show, using both retrieval simulations and validation data, that in many realistic conditions, the height of the Lambertian surface or the (middle) height of the scattering layer is in between the two scattering layers assumed in the simulation or somewhere inside the actual extinction profile measured, for example, with radar. Moreover, the retrieved height tends toward the height of the layer with the higher optical thickness or to the height with the highest extinction coefficient. Retrieved cloud pressures may then be interpreted as an average cloud pressure weighted, for example, by the contribution of each atmospheric layer to the top-of-atmosphere reflectance (see Joiner et al., 2012). Interestingly, however, for optically thin clouds or clouds with a small cloud fraction, the Lambertian surface can be retrieved above the actual cloud top height (see Wang and Stammes, 2014). For these clouds, as for aerosols, the contribution of the surface is large. We have discussed a possible mechanism that might explain why in our retrieval simulations the aerosol layer is retrieved above the elevated target layer when aerosols close to the surface are present and the surface albedo is fitted. Note at this point that the clustering of aerosol optical thicknesses in the right panel of Fig. 8 and particularly the decrease in magnitude of retrieved O_2 A band aerosol optical thicknesses compared to the left panel could be related to this mechanism (see the decrease of retrieved aerosol optical thickness in the right column of Fig. 15), but this needs to be further investigated. To conclude, optical thicknesses at the O_2 A band for boundary layer aerosol of about 0.1 are quite common and retrieved aerosol layer pressure can be significantly biased (Fig. 15) when the surface albedo is fitted.

Throughout all GOME-2A retrieval experiments, we have explicitly addressed the issue of stability of retrieval. By running retrievals for different sets of starting values for the fit (six in the case of the scene retrievals), we could estimate the dependence on starting values of both convergence and the retrieval solution. When the surface albedo is not fitted, 56 % of all GOME-2A pixels had at least one converging retrieval, and in fact, in that case retrievals for all starting values typically converged (i.e., the fraction of converged runs usually was either zero or one; not shown). When the surface albedo is fitted, 94 % of all GOME-2A pixels had at least one converging retrieval, but in this case, there is a dependence of convergence on starting values (i.e., the fraction of converged runs varied more smoothly between zero and one; not shown). In contrast to reports of multiple minima in the cost function observed in simulation studies (e.g., Hollstein et al., 2012; Sanders and De Haan, 2014), we find for the GOME-2A retrievals that multiple minima hardly seem to occur. Once retrieval converges, it typically converges to the same retrieval solution independent of starting values (see Fig. 9). Also, the average number of iterations needed for convergence is acceptable (3.9 when not fitting and 6.5 when fitting the surface albedo). The iterative scheme is based on Gauss–Newton iteration with two modifications to better account for possible non-linear behavior of the forward model. Because we presently have no clear indications that multiple minima in the cost function occur regularly, an efficient retrieval approach would be to attempt retrieval for different starting values until a run converges or a pre-defined maximum number of runs is reached. In the former case, it is assumed that the first converged run gives the global retrieval solution.

An important question in aerosol height retrieval is which aerosol model to assume. The simulation studies of Sect. 2 indicate that the retrieved height parameter (here the height of a scattering layer with constant particle extinction coefficient) is quite robust against model errors in the assumed aerosol type. This finding agrees with Hollstein and Fischer (2014), who show in a similar simulation study that the retrieved center height of a lognormal aerosol profile is also quite stable with respect to aerosol type. The simulations of Sect. 2 furthermore show that it helps in this respect to fit the surface albedo. Subsequent sensitivity experiments with GOME-2A spectra corroborate these findings. They show that the effect of the aerosol model is indeed modest, particularly when compared to other model errors and even when not fitting the surface albedo. This observation simplifies the retrieval problem considerably and it is the reason why at this

stage of algorithm development we do not give much priority to optimising the retrieval with respect to aerosol type.

In the selection of GOME-2A pixels, we have applied a strict filtering on clouds. The reason for doing so was twofold. First, we wanted to exclude pixels that are contaminated by cirrus to rule out that this might explain the low retrieved layer pressures. Second, since we are evaluating an aerosol height retrieval algorithm, we wanted to ensure that the scenes for which we investigate algorithm performance are truly aerosol scenes. Cloud filtering criteria can perhaps be more relaxed in the future. Considering the previous discussion of the effect of aerosol model, one could argue that our algorithm setup eventually is an algorithm optimised for retrieving the height of optically thin scattering layers, while a dedicated cloud retrieval algorithm such as SACURA is optimised for retrieving the height of optically thick scattering layers (e.g., with optical thicknesses larger than about five; Kokhanovsky and Rozanov, 2004). Thus, cloud contamination is not a fundamental problem from the perspective of algorithm performance per se.

We find that fit residuals have a distinct and systematic spectral structure. Previous case studies reporting residuals for retrievals comparable to ours include the studies by Van Diedenhoven et al. (2007) and Kokhanovsky and Rozanov (2010). Van Diedenhoven et al. (2007) present an improved method for cloud retrieval using O_2 A band measurements and simultaneous measurements in the UV. Their figure 15 depicts the mean and standard deviation of fit residuals at the O_2 A band for 3400 retrievals with GOME spectra. The study by Kokhanovsky and Rozanov (2010) has been discussed above. Their figure 11b depicts residuals for the single SCIAMACHY retrieval. Note that residuals in these two figures are defined as $(R_{\mathrm{fit}} - R_{\mathrm{meas}})/R \cdot 100\,\%$. Thus, they should be multiplied by -1 before they can be compared with ours. Overall, the residuals that these authors report are comparable in magnitude to the residuals shown in Fig. 11. The residuals also peak inside the deepest part of the O_2 A band, where they are about $8\,\% \pm 8\,\%$ (Van Diedenhoven et al., 2007) and about 16 % (Kokhanovsky and Rozanov, 2010). Residuals in the continuum near 758 nm in the left panel of Fig. 11 are perhaps somewhat larger than reported by these authors. Future research should look more closely into fit residuals and investigate to what model and instrument errors spectral characteristics of residuals can be traced back. In this respect, we mention uncertainties in the oxygen absorption cross section, including line-mixing effects and collision-induced absorptions. The improvement of convergence when the absorption cross section is scaled and a temperature offset is fitted as well as the observation that the retrieved temperature offset is systematically negative and quite large in that case supports the hypothesis that spectroscopic uncertainties may indeed be significant.

In the sensitivity experiments for the GOME-2A target pixels, we have also looked into the effect on retrieval of fitting stray light or fluorescence emissions. In both cases, no systematic improvement of convergence or residuals was found. At the same time, negative stray light offsets, meaning that light is removed from the radiance spectrum, and negative fluorescence emissions are found for both land and sea pixels. Therefore, we suspect that retrieved fluorescence emissions have the same origin as stray light offsets. Retrieval simulations in Sanders and De Haan (2013) indicate that fluorescence emissions may be fitted simultaneously with aerosol parameters with only a moderate loss of precision and accuracy of retrieved aerosol layer pressure. The spectral shape of fluorescence emission is known quite well, but for stray light this is not the case. The present experiment then indicates that it is needed in this respect that stray light is well characterised. For example, scenes free of clouds and aerosols may be identified to retrieve additive and multiplicative offsets including their spectral shape, provided the surface albedo and absorption cross sections are well known.

We adopted a fit window running from 758 to 770 nm. GOME-2A covers a much wider spectral range, so this fit window can in principle be complemented with other wavelengths to obtain more information about aerosols. However, inter-band and intra-band co-alignment errors will become more pronounced in that case. Alternatively, careful selection of channels at the O_2 A band (see Siddans et al., 2007) may be worth investigating in order to decrease the computation time.

Algorithm development may now proceed into two main directions. On the one hand, the retrieval simulations of Sect. 10 suggest that the retrieved height of an assumed single layer is most meaningful as a height parameter when the surface albedo is not fitted. In that case, however, the accuracy of the model for the surface reflectivity becomes more important. More effort should then be put into improving characterisation of the surface reflectivity. We have done some preliminary investigations using the ADAM-BRDF database (ESA, 2013). Perhaps a dynamic surface reflectance map (e.g., Sanghavi et al., 2010) rather than a monthly climatology based on multi-year averages can improve the retrieval. On the other hand, the retrieval simulations of Sect. 10 also suggest that the single-layer model does not adequately represent aerosol scattering near the surface in particular, leading to large biases if the surface albedo is fitted. Alternative profile parameterisations that better account for boundary layer aerosols, may ameliorate these biases. For example, one could try to fit optical thickness of a boundary layer with prescribed height in addition to the optical thickness and height of an elevated aerosol layer. The observation that residues increase and retrieved layer pressure decreases when boundary layer aerosols are added to the scene suggests that some information about boundary layer aerosols is contained in the spectrum. Alternatively, profile parameterisations using empirically determined orthogonal functions (e.g., Hollstein and Filipitsch, 2014) could also be worth investigating in this respect. In view of the limited information content, we strongly doubt however whether

adding many more profile parameters to the state vector will improve the retrieval. The problem of limited information is then merely shifted to finding better a priori information on aerosol profiles.

The main purpose of the TROPOMI Aerosol Layer Height product is to retrieve the height of localised aerosol layers in the free troposphere. Based on the results and the discussions presented in this paper, we currently (at the time of writing) decide to not fit the surface albedo in the operational baseline adopted for the Aerosol Layer Height product. Further efforts are taken to increase the computational speed of the algorithm. At this stage we prefer online calculations for their flexibility when improvements to the forward model are made. A correlated k-distribution method as described in Hasekamp and Butz (2008) is being implemented. At a later stage, efficient look-up table approaches, such as, for example, described in Hollstein and Lindstrot (2014), may be investigated.

Acknowledgements. This research has been funded in part by ESA's AEROPRO project (ESA Contract 4000105882/12/NL/MP) and the TROPOMI national program from the Netherlands Space Office (NSO).

We thank Rinus Scheele for performing calculations with the KNMI trajectory model TRAJKS, Philippe Le Sager for discussions on ECMWF data and Erwin Loots for discussions on many other aspects of this work (all are at KNMI). We thank Rüdiger Lang (EUMETSAT) for answering questions related to GOME-2A calibration, and Michael Grzegorski and other members from the PMAp team at EUMETSAT for processing and providing PMAp AOT data. Ben Veihelmann, Yasjka Meijer and Rob Koopman (ESA) are acknowledged for the many useful discussions and feedback during the AEROPRO project. Luca Lelli (IUP) is acknowledged for calculating expansion coefficients of the scattering matrix for the volcanic ash aerosol model.

We acknowledge the respective lidar teams for sharing their data. In particular, we thank Carmen Córdoba-Jabonero, Instituto Nacional de Técnica Aeroespacial (INTA), Madrid, Spain; Juan Luís Guerrero-Rascado, Andalusian Center for Environmental Research (CEAMA), Granada, Spain; Frank Wagner, Deutscher Wetterdienst (DWD), Germany and University of Evora, Portugal; Vassilis Amiridis, National Observatory of Athens (NOA), Greece; Mariliza Koukouli, Aristotle University of Thessaloniki, Greece; Franco Marenco, UK Met Office, UK; Dave Donovan, KNMI.

AVHRR cloud mask data that we used in initial stages of the project, were provided by EUMETSAT's Satellite Application Facility on Climate Monitoring (CM SAF). Meteorological data were taken from ECMWF's ERA Interim project. EUMETSAT is acknowledged for making available GOME-2A level-1b and PMAp data. The AAI is provided by EUMETSAT's Satellite Application Facility for Atmospheric Composition and UV Radiation (O3M SAF). The AERONET and MODIS teams are acknowledged for making available their aerosol data. Ground-based lidar measurements from EARLINET and MPLNET stations, airborne measurements aboard the FAAM aircraft jointly owned by NERC and UKMO, and spaceborne measurements from CALIPSO were used. We read BRDF data from ESA's ADAM database. Finally, a Fortran 77 code for line-mixing in the O_2 A band, including the updates discussed in Tran and Hartmann (2008), was provided by J.-M. Hartmann.

Edited by: J. Kim

References

Amoros-Lopez, J., Gomez-Chova, L., Vila-Frances, J., Alonso, L., Calpe, J., Moreno, J., and Del Valle-Tascon, S.: Evaluation of remote sensing of vegetation fluorescence by the analysis of diurnal cycles, Int. J. Remote Sens., 29, 17–18, 5423–5436, doi:10.1080/01431160802036391, 2008.

Butz, A., Guerlet, S., Hasekamp, O. P., Kuze, A., and Suto, H.: Using ocean-glint scattered sunlight as a diagnostic tool for satellite remote sensing of greenhouse gases, Atmos. Meas. Tech., 6, 2509–2520, doi:10.5194/amt-6-2509-2013, 2013.

Chance, K. and Kurucz, R. L.: An improved high-resolution solar reference spectrum for earth's atmosphere measurements in the ultraviolet, visible, and near infrared, J. Quant. Spectrosc. Ra., 111, 1289–1295, doi:10.1016/j.jqsrt.2010.01.036, 2010.

Corradini, S. and Cervino, M.: Aerosol extinction coefficient profile retrieval in the oxygen A-band considering multiple scattering atmosphere. Test case: SCIAMACHY nadir simulated measurements, J. Quant. Spectrosc. Ra., 97, 354–380, doi:10.1016/j.jqsrt.2005.05.061, 2006.

Crisp, D., Fisher, B. M., O'Dell, C., Frankenberg, C., Basilio, R., Bösch, H., Brown, L. R., Castano, R., Connor, B., Deutscher, N. M., Eldering, A., Griffith, D., Gunson, M., Kuze, A., Mandrake, L., McDuffie, J., Messerschmidt, J., Miller, C. E., Morino, I., Natraj, V., Notholt, J., O'Brien, D. M., Oyafuso, F., Polonsky, I., Robinson, J., Salawitch, R., Sherlock, V., Smyth, M., Suto, H., Taylor, T. E., Thompson, D. R., Wennberg, P. O., Wunch, D., and Yung, Y. L.: The ACOS CO_2 retrieval algorithm – Part II: Global XCO_2 data characterization, Atmos. Meas. Tech., 5, 687–707, doi:10.5194/amt-5-687-2012, 2012.

De Graaf, M., Stammes, P., Torres, O., and Koelemeijer, R. B. A.: Absorbing Aerosol Index: sensitivity analysis, application to GOME and comparison with TOMS, J. Geophys. Res., 110, D01201, doi:10.1029/2004JD005178, 2005.

De Haan, J. F, Bosma, P. B., and Hovenier, J. W.: The adding method for multiple scattering calculations of polarized light, Astron. Astrophys., 183, 371–391, 1987.

De Leeuw, G., Holzer-Popp, T., Bevan, S., Davies, W., Descloitres, J., Grainger, R. G., Griesfeller, J., Heckel, A., Kinne, S., Klüser, L., Kolmonen, P., Litvinov, P., Martynenko, D., North, P., Ovigneur, B., Pascal, N., Poulsen, C., Ramon, D., Schulz, M., Siddans, R., Sogacheva, L., Tanré, D., Thomas, G. E., Virtanen, T. H., Von Hoyningen Huene, W., Vountas, M., and Pinnock, S.: Evaluation of seven European aerosol optical depth retrieval algorithms for climate analysis, Remote Sens. Environ., 162, 295–315, 2015.

Dirksen, R. J., Boersma, K. F., De laat, J., Stammes, P., Van der Werf, G. R., Val Martin, M., and Kelder, H. M.: An aerosol boomerang: rapid around-the-world transport of smoke from the December 2006 Australian forest fires observed from space, J. Geophys. Res., 114, D21201, doi:10.1029/2009JD012360, 2009.

Dubovik, O., Holben, B., Eck, T. F., Smirnov, A., Kaufman, Y. J., King, M. D., Tanré, D., and Slutsker, I.: Variability of absorption and optical properties of key aerosol types observed in worldwide locations, J. Atmos. Sci., 59, 590–608, 2002.

Dubuisson, P., Frouin, R., Dessailly, D., Duforêt, L., Léon, J.-F., Voss, K., and Antoine, D.: Estimating the altitude of aerosol plumes over the ocean from reflectance ratio measurements in the O_2 A-band, Remote Sens. Environ., 113, 1899–1911, doi:10.1016/j.rse.2009.04.018, 2009.

European Organisation for the Exploitation of Meteorological Satellites (EUMETSAT): AVHRR Level 1b Product Guide, EUM/OPS-EPS/MAN/04/0029, issue v3A, 21 January 2011, EUMETSAT, Darmstadt, Germany, available at: http://www.eumetsat.int/website/home/Data/TechnicalDocuments/index.html (last access: 6 November 2014), 2011.

European Organisation for the Exploitation of Meteorological Satellites (EUMETSAT): GOME-2 Factsheet, EUM/OPS/DOC/10/1299, issue v4A, 20 May 2014, EUMETSAT, Darmstadt, Germany, available at: http://www.eumetsat.int/website/home/Data/TechnicalDocuments/index.html (last access: 25 October 2014), 2014a.

European Organisation for the Exploitation of Meteorological Satellites (EUMETSAT): Polar Multi-Sensor Aerosol Product: ATBD, EUM/TSS/SPE/14/739904, issue v2D, 21 May 2014, EUMETSAT, Darmstadt, Germany, available at: http://www.eumetsat.int/website/home/Data/TechnicalDocuments/index.html (last access: 6 November 2014), 2014b.

European Organisation for the Exploitation of Meteorological Satellites (EUMETSAT): Polar Multi-Sensor Aerosol Product: Validation Report, EUM/TSS/REP/14/745438, issue v1A, 3 March 2014, EUMETSAT, Darmstadt, Germany, available at: http://www.eumetsat.int/website/home/Data/TechnicalDocuments/index.html (last access: 23 December 2014), 2014c.

European Space Agency (ESA): GMES Sentinels 4 and 5 Mission Requirements Traceability Document, issue 1, 20 September 2012, ESTEC, Noordwijk, the Netherlands, available at: http://esamultimedia.esa.int/docs/EarthObservation/S4_5_5p_MRTD_issue_1.0_authorised.pdf (last access: 26 March 2013), 2012.

European Space Agency (ESA): A Surface Reflectance DAtabase for ESA's Earth Observation Missions (ADAM): Improvement and/or Expansion of Existing Surface Datasets – Algorithm Theoretical Basis Document, issue 2-1, 2 September 2013, ESTEC, Noordwijk, the Netherlands, available at: http://adam.noveltis.com/pdfs/NOV-3895-NT-12121_TN4_v2.1.pdf (last access: 11 January 2015), 2013.

Fishman, J., Iraci, L. T., Al-Saadi, J., Chance, K., Chavez, F., Chin, M., Coble, P., Davis, C., DiGiacomo, P. M., Edwards, D., Eldering, A., Goes, J., Herman, J., Hu, C., Jacob, D. J, Jordan, C., Kawa, S. R., Key, R., Liu, X., Lohrenz, S., Mannino, A., Natraj, V., Neil, D., Neu, J., Newchurch, M., Pickering, K., Salisbury, J., Sosik, H., Subramaniam, A., Tzortziou, M., Wang, J. and Wang, M.: The United States' next generation of atmospheric composition and coastal ecosystem measurements: NASA's Geostationary Coastal and Air Pollution Events (GEO-CAPE) mission, Bull. Amer. Meteor. Soc., 93, 1547–1566, doi:10.1175/BAMS-D-11-00201.1, 2012.

Gabella, M., Kisselev, V., and Perona, G.: Retrieval of aerosol profile variations from reflected radiation in the oxygen absorption A band, Appl. Optics, 38, 3190–3195, 1999.

Geddes, A. and Bösch, H.: Tropospheric aerosol profile information from high-resolution oxygen A-band measurements from space, Atmos. Meas. Tech., 8, 859–874, doi:10.5194/amt-8-859-2015, 2015.

Hasekamp, O. P. and Butz, A.: Efficient calculation of intensity and polarization spectra in vertically inhomogeneous scattering and absorption atmospheres, J. Geophys. Res., 113, D20309, doi:10.1029/2008JD010379, 2008.

Hasekamp, O. and Siddans, R.: Aerosols, Chapt. 8, in: CAMELOT Task 3 Report – Retrieval simulations, edited by: Veefkind, J. P., ESA Contract No. 21533/07/NL/HE, issue 1, 30 November 2009, ESTEC, Noordwijk, the Netherlands, 269–310, 2009.

Hollstein, A. and Filipitsch, F.: Global representation of aerosol vertical profiles by sums of lognormal modes: consequences for the passive remote sensing of aerosol heights, J. Geophys. Res.-Atmos., 119, 8899–8907, doi:10.1002/2014JD021472, 2014.

Hollstein, A. and Fischer, J.: Retrieving aerosol height from the oxygen A band: a fast forward operator and sensitivity study concerning spectral resolution, instrumental noise, and surface inhomogeneity, Atmos. Meas. Tech., 7, 1429–1441, doi:10.5194/amt-7-1429-2014, 2014.

Hollstein, A. and Lindstrot, R.: Fast reconstruction of hyperspectral radiative transfer simulations by using small spectral subsets: application to the oxygen A band, Atmos. Meas. Tech., 7, 599–607, doi:10.5194/amt-7-599-2014, 2014.

Hollstein, A., Lindstrot, R., and Fischer, J.: Retrieval of Aerosol Vertical Profile from Top of Atmosphere and High Spectral Resolution Radiance Measurements in the O_2 A Band, Technical Note within the Atmospheric Corrections for Fluorescence Signal Retrieval (FLUSS) project, ESA Contract No. 4000102733/11/NL/AF, ESTEC, Noordwijk, the Netherlands, 2012.

Hovenier, J. W., Van der Mee, C. V. M., and Domke, H.: Transfer of Polarized Light in Planetary Atmospheres; Basic Concepts and Practical Methods, Kluwer, Dordrecht, the Netherlands, 2004.

Illingworth, A. J., Barker, H. W., Beljaars, A., Ceccaldi, M., Chepfer, H., Cole, J., Delanoë, J., Domenech, C., Donovan, D. P., Fukuda, S., Hirakata, M., Hogan, R. J., Huenerbein, A., Kollias, P., Kubota, T., Nakajima, T., Nakajima, T. Y., Nishizawa, T., Ohno, Y., Okamoto, H., Oki, R., Sato, K., Satoh, M., Shephard, M., Wandinger, U., Wehr, T., and Zadelhoff, G.-J.: The EarthCARE satellite: the next step forward in global measurements of clouds, aerosols, precipitation and radiation, B. Am. Meteorol. Soc., doi:10.1175/BAMS-D-12-00227.1, online first, 2014.

Johnson, B., Turnbull, K., Brown, P., Burgess, R., Dorsey, J., Baran, A. J., Webster, H., Haywood, J., Cotton, R., Ulanowski, Z., Hesse, E., Woolley, A., and Rosenberg, P.: In situ observations of volcanic ash clouds from the FAAM aircraft during the eruption of Eyjafjallajökull in 2010, J. Geophys. Res., 117, D00U24, doi:10.1029/2011JD016760, 2012.

Joiner, J., Vasilkov, A. P., Bhartia, P. K., Wind, G., Platnick, S., and Menzel, W. P.: Detection of multi-layer and vertically-extended

clouds using A-train sensors, Atmos. Meas. Tech., 3, 233–247, doi:10.5194/amt-3-233-2010, 2010.

Joiner, J., Vasilkov, A. P., Gupta, P., Bhartia, P. K., Veefkind, P., Sneep, M., de Haan, J., Polonsky, I., and Spurr, R.: Fast simulators for satellite cloud optical centroid pressure retrievals; evaluation of OMI cloud retrievals, Atmos. Meas. Tech., 5, 529–545, doi:10.5194/amt-5-529-2012, 2012.

Kahn, R. A., Li, W.-H., Moroney, C., Diner, D. J., Martonchik, J. V., and Fishbein, E.: Aerosol source plume physical characteristics from space-based multiangle imaging, J. Geophys. Res., 112, D11205, doi:10.1029/2006JD007647, 2007.

Koelemeijer, R. B. A., Stammes, P., Hovenier, J. W., and De Haan, J. F.: A fast method for retrieval of cloud parameters using oxygen A band measurements from the Global Ozone Monitoring Experiment, J. Geophys. Res., 106, 3475–3490, 2001.

Koelemeijer, R. B. A., Stammes, P., Hovenier, J. W., and De Haan, J. F.: Global distributions of effective cloud fraction and cloud top pressure derived from oxygen A band spectra measured by the Global Ozone Monitoring Experiment: comparison to ISCCP data, J. Geophys. Res., 107, AAC 5-1–AAC 5-9, doi:10.1029/2001JD000840, 2002.

Koelemeijer, R. B. A., De Haan, J. F., and Stammes, P.: A database of spectral surface reflectivity in the range 335–772 nm derived from 5.5 years of GOME observations, J. Geophys. Res., 108, D24070, doi:10.1029/2002JD002429, 2003.

Kokhanovsky, A. A. and Rozanov, V. V.: The physical parameterization of the top-of-atmosphere reflection function for a cloudy atmosphere–underlying surface system: the oxygen A-band case study, J. Quant. Spectrosc. Ra., 85, 35–55, doi:10.1016/S0022-4073(03)00193-6, 2004.

Kokhanovsky, A. A. and Rozanov, V. V.: The determination of dust cloud altitudes from a satellite using hyperspectral measurements in the gaseous absorption band, Int. J. Remote Sens., 31, 2729–2744, doi:10.1080/01431160903085644, 2010.

Kokhanovsky, A. A., Rozanov, V. V., Nauss, T., Reudenbach, C., Daniel, J. S., Miller, H. L., and Burrows, J. P.: The semianalytical cloud retrieval algorithm for SCIAMACHY I. The validation, Atmos. Chem. Phys., 6, 1905–1911, doi:10.5194/acp-6-1905-2006, 2006a.

Kokhanovsky, A. A., von Hoyningen-Huene, W., Rozanov, V. V., Noël, S., Gerilowski, K., Bovensmann, H., Bramstedt, K., Buchwitz, M., and Burrows, J. P.: The semianalytical cloud retrieval algorithm for SCIAMACHY II. The application to MERIS and SCIAMACHY data, Atmos. Chem. Phys., 6, 4129–4136, doi:10.5194/acp-6-4129-2006, 2006b.

Koppers, G. A. A., and Murtagh, D. P.: Retrieval of height resolved aerosol optical thickness in the atmospheric band, Chapt. 5, in: Radiative Transfer in the Absorption Bands of Oxygen: Studies of their Significance in Ozone Chemistry and Potential for Aerosol Remote Sensing, edited by: Koppers, G. A. A., Stockholm University, Stockholm, Sweden, 1–24, 1997.

Landgraf, J., Hasekamp, O., Box, M., and Troutmann, T.: A linearized radiative transfer model for ozone profile retrieval using the analytical forward-adjoint perturbation approach, J. Geophys. Res., 106, 27291–27305, 2001.

Lelli, L., Kokhanovsky, A. A., Rozanov, V. V., Vountas, M., Sayer, A. M., and Burrows, J. P.: Seven years of global retrieval of cloud properties using space-borne data of GOME, Atmos. Meas. Tech., 5, 1551–1570, doi:10.5194/amt-5-1551-2012, 2012.

Lelli, L., Kokhanovsky, A. A., Rozanov, V. V., Vountas, M., and Burrows, J. P.: Linear trends in cloud top height from passive observations in the oxygen A-band, Atmos. Chem. Phys., 14, 5679–5692, doi:10.5194/acp-14-5679-2014, 2014.

Lelli, L. et al.: Science verification of aerosol layer height for Sentinel-5 Precursor: a multi-sensor volcanic case study, in preparation, 2016.

Loyola, D. G., Thomas, W., Livschitz, Y., Ruppert, T., Albert, P., and Hollmann, R.: Cloud properties derived from GOME/ERS-2 backscatter data for trace gas retrieval, IEEE T. Geosci. Remote, 45, 2747–2758, doi:10.1109/TGRS.2007.901043, 2007.

Mona, L., Pappalardo, G., Amodeo, A., D'Amico, G., Madonna, F., Boselli, A., Giunta, A., Russo, F., and Cuomo, V.: One year of CNR-IMAA multi-wavelength Raman lidar measurements in coincidence with CALIPSO overpasses: Level 1 products comparison, Atmos. Chem. Phys., 9, 7213–7228, doi:10.5194/acp-9-7213-2009, 2009.

Muñoz, O., Volten, H., de Haan, J. F., Vassen, W., and Hovenier, J. W.: Experimental determination of the phase function and degree of linear polarization of El Chichòn and Pinatubo volcanic ashes, J. Geophys. Res., 107, ACL 4-1–ACL 4-8, doi:10.1029/2001JD000983, 2002.

Muñoz, O., Volten, H., Hovenier, J. W., Veihelmann, B., van der Zande, W. J., Waters, L. B. F. M., and Rose, W. I.: Scattering matrices of volcanic ash particles of Mount St. Helens, Redoubt, and Mount Spurr Volcanoes, J. Geophys. Res., 109, D16201, doi:10.1029/2004JD004684, 2004.

Muñoz, O., Moreno, F., Guirado, D., Dabrowska, D. D., Volten, H., and Hovenier, J. W.: The Amsterdam – Granada Light Scattering Database, J. Quant. Spectrosc. Ra., 113, 565–574, doi:10.1016/j.jqsrt.2012.01.014, 2012.

Nelson, D. L., Chen, Y., Kahn, R. A., Diner, D. J., and Mazzoni, D.: Example applications of the MISR INteractive eXplorer (MINX) software tool to wildfire smoke plume analyses, Proc. SPIE, 7089, 708909, doi:10.1117/12.795087, 2008.

Pappalardo, G., Wandinger, U., Mona, L., Hiebsch, A., Mattis, I., Amodeo, A., Ansmann, A., Seifert, P., Linné, H., Apituley, A., Alados Arboledas, L., Balis, D., Chaikovsky, A., D'Amico, G., De Tomasi, F., Freudenthaler, V., Giannakaki, E., Giunta, A., Grigorov, I., Iarlori, M., Madonna, F., Mamouri, R.-E., Nasti, L., Papayannis, A., Pietruczuk, A., Pujadas, M., Rizi, V., Rocadenbosch, F., Russo, F., Schnell, F., Spinelli, N., Wang, X., and Wiegner, M.: EARLINET correlative measurements for CALIPSO: first intercomparison results, J. Geophys. Res., 115, D00H19, doi:10.1029/2009JD012147, 2010.

Pappalardo, G., Amodeo, A., Apituley, A., Comeron, A., Freudenthaler, V., Linné, H., Ansmann, A., Bösenberg, J., D'Amico, G., Mattis, I., Mona, L., Wandinger, U., Amiridis, V., Alados-Arboledas, L., Nicolae, D., and Wiegner, M.: EARLINET: towards an advanced sustainable European aerosol lidar network, Atmos. Meas. Tech., 7, 2389–2409, doi:10.5194/amt-7-2389-2014, 2014.

Popp, C., Wang, P., Brunner, D., Stammes, P., Zhou, Y., and Grzegorski, M.: MERIS albedo climatology for FRESCO+ O2 A-band cloud retrieval, Atmos. Meas. Tech., 4, 463–483, doi:10.5194/amt-4-463-2011, 2011.

Preißler, J., Wagner, F., Pereira, S. N., and Guerrero-Rascado, J. L.: Multi-instrumental observation of an exceptionally strong Saha-

ran dust outbreak over Portugal, J. Geophys. Res., 116, D24204, doi:10.1029/2011JD016527, 2011.

Rodgers, C. D.: Inverse Methods for Atmospheric Sounding: Theory and Practice, World Scientific Publishing, Singapore, 240 pp., 2000.

Rozanov, V. V. and Kokhanovsky, A. A.: Semianalytical cloud retrieval algorithm as applied to the cloud top altitude and the cloud geometrical thickness determination from top-of-atmosphere reflectance measurements in the oxygen A band, J. Geophys. Res., 109, D05202, doi:10.1029/2003JD004104, 2004.

Sanders, A. F. J. and de Haan, J. F.: Retrieval of aerosol parameters from the oxygen A band in the presence of chlorophyll fluorescence, Atmos. Meas. Tech., 6, 2725–2740, doi:10.5194/amt-6-2725-2013, 2013.

Sanders, A. F. J. and De Haan, J. F.: TROPOMI ATBD of the Aerosol Layer Height product, S5P-KNMI-L2-0006-RP, issue 0.11.0 (in review), 30 September 2014, KNMI, De Bilt, the Netherlands, 2014.

Sanghavi, S., Platt, U., and Landgraf, J.: Bichromatic method for identification of clear-sky scenarios over ground pixel viewed from space, Appl. Optics, 49, 3282–3290, 2010.

Sanghavi, S., Martonchik, J. V., Landgraf, J., and Platt, U.: Retrieval of the optical depth and vertical distribution of particulate scatterers in the atmosphere using O_2 A- and B-band SCIAMACHY observations over Kanpur: a case study, Atmos. Meas. Tech., 5, 1099–1119, doi:10.5194/amt-5-1099-2012, 2012.

Schumann, U., Weinzierl, B., Reitebuch, O., Schlager, H., Minikin, A., Forster, C., Baumann, R., Sailer, T., Graf, K., Mannstein, H., Voigt, C., Rahm, S., Simmet, R., Scheibe, M., Lichtenstern, M., Stock, P., Rüba, H., Schäuble, D., Tafferner, A., Rautenhaus, M., Gerz, T., Ziereis, H., Krautstrunk, M., Mallaun, C., Gayet, J.-F., Lieke, K., Kandler, K., Ebert, M., Weinbruch, S., Stohl, A., Gasteiger, J., Groß, S., Freudenthaler, V., Wiegner, M., Ansmann, A., Tesche, M., Olafsson, H., and Sturm, K.: Airborne observations of the Eyjafjalla volcano ash cloud over Europe during air space closure in April and May 2010, Atmos. Chem. Phys., 11, 2245–2279, doi:10.5194/acp-11-2245-2011, 2011.

Siddans, R., Kerridge, B. J., Latter, B. G., Smeets, J., and Otter, G.: Analysis of GOME-2 Slit function Measurements, EUMETSAT Contract no. EUM/CO/04/1298/RM, 9 March 2006, EUMETSAT, Darmstadt, Germany, 2006.

Siddans, R., Latter, B. G., and Kerridge, B. J.: Study to Consolidate the UVS Mission Requirements for the Oxygen A-band, EUMETSAT Contract No. EUM/CO/05/1411/SAT, issue 1.2, 24 May 2007, EUMETSAT, Darmstadt, Germany, 2007.

Sneep, M., De Haan, J. F., Stammes, P., Wang, P., Vanbauce, C., Joiner, J., Vasilkov, A. P., and Levelt, P. F.: Three-way comparison between OMI and PARASOL cloud pressure products, J. Geophys. Res., 113, D15S23, doi:10.1029/2007JD008694, 2008.

Timofeyev, Y. M., Vasilyev, A. V., and Rozanov, V. V.: Information content of the spectral measurements of the 0.76 µm O_2 outgoing radiation with respect to the vertical aerosol optical properties, Adv. Space Res., 16, 1091–1094, 1995.

Tran, H. and Hartmann, J.-M.: An improved O_2 A band absorption model and its consequences for retrievals of photon paths and surface pressure, J. Geophys. Res., 113, D18104, doi:10.1029/2008JD010011, 2008.

Tran, H., Boulet, C., and Hartmann, J.-M.: Line mixing and collision-induced absorption by oxygen in the A band: laboratory measurements, model, and tools for atmospheric spectra computations, J. Geophys. Res., 111, D15210, doi:10.1029/2005JD006869, 2006.

Val Martin, M., Logan, J. A., Kahn, R. A., Leung, F.-Y., Nelson, D. L., and Diner, D. J.: Smoke injection heights from fires in North America: analysis of 5 years of satellite observations, Atmos. Chem. Phys., 10, 1491–1510, doi:10.5194/acp-10-1491-2010, 2010.

Van Diedenhoven, B., Hasekamp, O.P, and Landgraf, J.: Retrieval of cloud parameters from satellite-based reflectance measurements in the ultraviolet and the oxygen A-band, J. Geophys. Res., 112, D15208, doi:10.1029/2006JD008155, 2007.

Van Weele, M., Levelt, P., Aben, I., Veefkind, P., Dobber, M., Eskes, H., Houweling, S., Landgraf, J., and Noordhoek, R.: Science Requirements Document for TROPOMI, Volume I: Mission and Science Objectives and Observational Requirements, RS-TROPOMI-KNMI-017, issue 2.0, 30 October 2008, KNMI, De Bilt, the Netherlands, 2008.

Vasilkov, A., Joiner, J., Spurr, R., Bhartia, P. K., Levelt, P., and Stephens, G.: Evaluation of the OMI cloud pressures derived from rotational Raman scattering by comparisons with other satellite data and radiative transfer simulations, J. Geophys. Res., 113, D15S19, doi:10.1029/2007JD008689, 2008.

Veefkind, J. P., Aben, I., McMullan, K., Förster, H., De Vries, J., Otter, G., Claas, J., Eskes, H. J., De Haan, J. F., Kleipool, Q., Van Weele, M., Hasekamp, O., Hoogeveen, R., Landgraf, J., Snel, R., Tol, P., Ingmann, P., Voors, R., Kruizinga, B., Vink, R., Visser, H., and Levelt, P. F.: TROPOMI on the ESA Sentinel-5 Precursor: a GMES mission for global observations of the atmospheric composition for climate, air quality and ozone layer applications, Remote Sens. Environ., 120, 70–83, doi:10.1016/j.rse.2011.09.027, 2012.

Volten, H., Muñoz, O., Rol, E., de Haan, J. F., Vassen, W., Hovenier, J. W., Muinonen, K., and Nousiainen, T.: Scattering matrices of mineral particles at 441.6 nm and 632.8 nm, J. Geophys. Res., 106, 17375–17401, 2001.

Wang, P. and Stammes, P.: Evaluation of SCIAMACHY Oxygen A band cloud heights using Cloudnet measurements, Atmos. Meas. Tech., 7, 1331–1350, doi:10.5194/amt-7-1331-2014, 2014.

Wang, P., Stammes, P., van der A, R., Pinardi, G., and van Roozendael, M.: FRESCO+: an improved O_2 A-band cloud retrieval algorithm for tropospheric trace gas retrievals, Atmos. Chem. Phys., 8, 6565–6576, doi:10.5194/acp-8-6565-2008, 2008.

Wang, P., Tuinder, O. N. E., Tilstra, L. G., de Graaf, M., and Stammes, P.: Interpretation of FRESCO cloud retrievals in case of absorbing aerosol events, Atmos. Chem. Phys., 12, 9057–9077, doi:10.5194/acp-12-9057-2012, 2012.